Trajectory Modelling of Transition Regime Using Blade Element Method for Different eVTOL Aircraft Configurations

Shawn Lim Kin Yip
PhD Candidate
kinyipsh001@e.ntu.edu.sg
Nanyang Technological University
Singapore

Boon Zhi Yuan
Research Assistant
boon0025@e.ntu.edu.sg
Nanyang Technological University
Singapore

James Wang
Professor
james.wang@ntu.edu.sg
Nanyang Technological University
Singapore

ABSTRACT

With the rising popularity of Electric Vertical Take Off and Landing (eVTOL) aircraft, there is a proliferation of numerous works on the different eVTOL designs with configurations such as vectored thrust, lift + cruise and multicopter. However, there are limited published studies focusing on the characteristics of transition flight for different eVTOL aircraft configurations. This paper investigates the generation and derivation of the complete eVTOL aircraft transition model based on both the transitional flight trajectory and power requirements. Different modelling modules using the eVTOL aircraft flight trajectory are developed and integrated within MATLAB, including the use of Blade Element Momentum Theory in the power required module. In addition, a generalized trim module determines the balanced forces and moments acting on the eVTOL aircraft. In the kinematic module, the trajectory model accounts for the dynamic and transient conditions during the transition phase. These modules enables the study of the full transition regime for any eVTOL aircraft and is applicable for different eVTOL configurations, including tiltrotors. The estimation of the transitional power required for these eVTOL aircraft for given a transition trajectory, allows for proper motor and energy battery sizing. This research benefits the aircraft designers and the eVTOL industry to deepen the understanding of the transition regime for eVTOL aircraft.

NOTATION

eVTOL Dimensions

ρ	eVTOL aircraft mass
$\mathrm{m_{eVTOL}}$	eVTOL aircraft mass [kg]
$\mathrm{W_{eVTOL}}$	eVTOL aircraft weight [N]
S	Wing area [m^2]
AR	Wing aspect ratio
x_i	Rotor location from CG in x-axis [m]
$\mathrm{y_i}$	Rotor location from CG in y-axis [m]
$\mathrm{z_i}$	Rotor location from CG in z-axis [m]

Rotor Dimensions

R	Radius of rotor [m]
c	Rotor blade chord length [m]
ΩR	Rotor tip speed [m/s]
κ	BEMT correction factor
C_{d_0}	Rotor blade drag coefficient
N	Number of rotors
σ	Rotor solidity
τ	Shaft Angle [°]
T	Thrust required [N]
$T_{x_{rotor_i}}$	Rotor thrust required in x-axis [N]
$T_{y_{rotor_i}}$	Rotor thrust required in y-axis [N]
$T_{z_{rotor_i}}$	Rotor thrust required in z-axis [N]
R	Radius of rotor [m]
c	Rotor blade chord length [m]
ΩR	Rotor tip speed [m/s]

Power Requirement

P_{req}	Total Power Required [kW]
$P_{induced}$	Total Induced Power [kW]
$P_{profile}$	Total Profile Power [kW]
P_{net}	Total Motion Power [kW]
C_P	Normalized Power Required
$C_{P_{induced}}$	Normalized Induced Power
$C_{P_{profile}}$	Normalized Profile Power
$C_{P_{net}}$	Normalized Motion Power
λ	Inflow Ratio
λ_{net}	Motion Inflow Ratio
μ	Advance Ratio

Force and Moment

F_x	Force in x-axis [N]
F_y	Force in y-axis [N]
F_z	Force in z-axis [N]
M_{x_i}	Moments about x-axis [Nm]
M_{y_i}	Moments about y-axis [Nm]
M_{z_i}	Moments about z-axis [Nm]
V_{∞_z}	Velocity in the z-axis [m/s]
V_{∞_x}	Velocity in the x-axis [m/s]
$\mathrm{V_{net}}$	Resultant Velocity [m/s]
γ	Climb/Descent Angle [°]
α_{eff}	Effective angle of attack [°]
θ	Pitch Angle [°]
C_{L_α}	Gradient of lift coefficient curve
C_{D_α}	Gradient of drag coefficient curve
C_{D_0}	Parasite drag coefficient

$C_{D_{Fuselage}}$	Fuselage drag coefficient
L_{wing}	Lift generated by wing [N]
D_{wing}	Drag generated by wing [N]
e	Oswald efficiency number

Kinematic and Trajectory

F_i	Resultant force vector in each axis [N]
a_i	Acceleration in each axis [m/s^2]
S_z	Vertical displacement [m]
V_z	Vertical velocity [m/s]
a_s	Vertical acceleration [m/s^2]
S_x	Horizontal displacement [m]
V_x	Horizontal velocity [m/s]
a_x	Horizontal acceleration [m/s^2]

1. INTRODUCTION

Due to high congestion in populated cities around the world, this has led to the evolution towards new transportation systems in the urban regions. In recent years, there is an increase in popularity of Electric Vertical Take Off and Landing (eVTOL) aircraft with different configurations that can vertically take off and then transition into forward flight such as Lift + Cruise, Tiltrotor and Lift + Tiltrotor as shown in

Table 8. However, depending on the eVTOL configuration, the aircraft in stationary hover position may require pitching its nose downward to gain forward airspeed during transition. Only until the eVTOL airspeed is above the stall speed, then a complete wing borne forward flight can be achieved.

An example of a generic eVTOL aircraft with tiltable front rotors and its different phases from a stationary hover to a full forward flight are shown in Figure 1. In the transition segment, there are 2 possible types of transition trajectories: (1) unlevelled and (2) levelled. In (1), it is similar to a helicopter and multicopters, where the aircraft pitches its nose downward initially to accelerate and gain forward flight speed then tilting its front rotors forward as shown in Figure 2 (a).

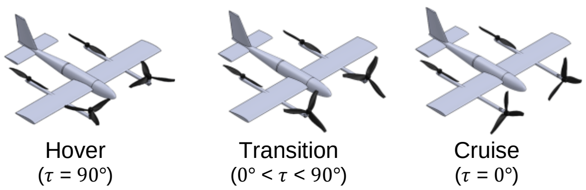

Figure 1 eVTOL Aircraft different phases during transition.

(a): Unlevelled transition trajectory

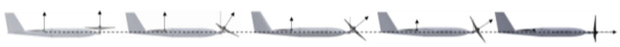

(b): Levelled transition trajectory

Figure 2 Different types of eVTOL transition trajectories

In (2), the aircraft maintains its fuselage in a level attitude and then tilt the front rotors forward to building up airspeed, as shown in Figure 2 (b). All eVTOL aircraft have a band for its transition corridor profile to transition from hover into forward flight.

In the transition segment, kinematic properties and aerodynamic forces are constantly changing for each state of flight. Furthermore, due to different eVTOL aircraft designs with different configurations such as tiltrotors or different sets of rotors/propellers, the transition conditions between hover and cruise are unique to each configuration. This highlights an optimal transition trajectory between hover and cruise for each eVTOL aircraft for a given design and its power and energy system. As such the two main parameters in the transition regime that are the power requirement and the desired trajectory. Therefore, emphasizing a need to investigate the transition characteristics for different eVTOL configuration, in order to find the desired transition trajectory and to allow for the optimal motor and energy system sizing based on the calculated power required.

In 2023, EASA has published a technical requirement in the Special Condition VTOL document for the safe operation of eVTOL aircraft [1], with a performance objective for both the basic and enhanced categories with various take-off profiles such as Elevated Conventional Take-off, Conventional Take-off, Vertical Take-off, as shown in Figure 3. The operating trajectory must be determined for both controlled emergency landings (CEL) for basic category or continued safe flight and landing (CSFL) for enhanced category. Furthermore, the trajectory analysis is required to determine the size of the funnel shaped take-off volume with safety area to prevent collision with obstacles. EASA grants the flexibility to aircraft manufacturer to demonstrate during their certification process that their aircraft can operate within the designated volume. Thus, a transitional trajectory analysis is required for the means of eVTOL certification.

The trajectories of eVTOL aircraft are essential for their certification, as it affects the operations and implementation of eVTOL aircraft over urban areas as well as to determine the locations of vertiports for taking off and landing of the aircraft. Hence, the aircraft trajectories help to regulate the take-off and landing for maximum flexibility for aircraft pilots and manufacturers as well as the effects of both the power and energy requirements during its mission. In addition, eVTOL aircraft trajectory studies can be expanded to include the effects of interferences such as obstacles and for failure trajectories in case of emergencies for non-scheduled landings.

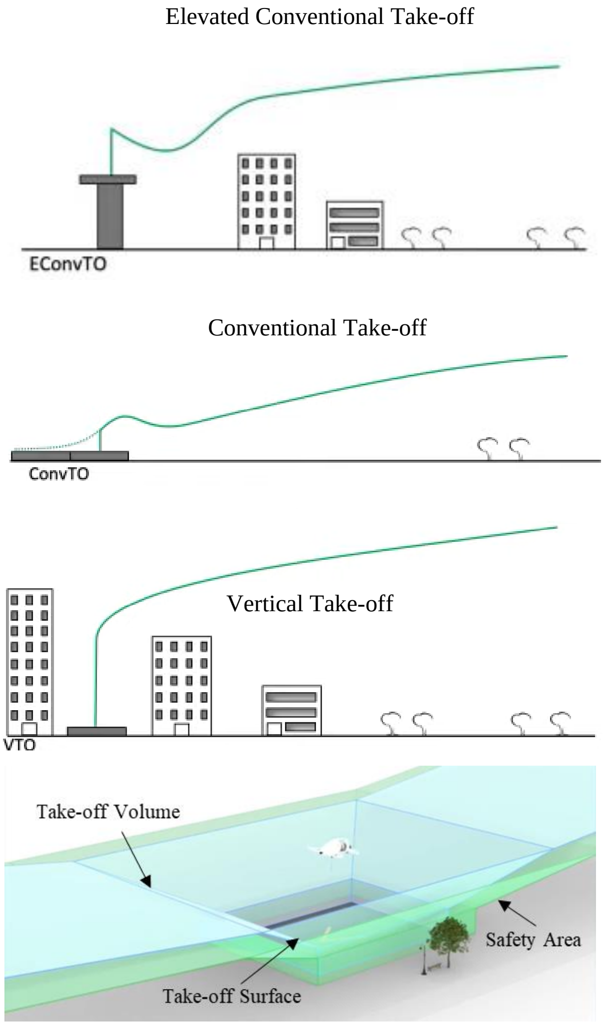

Figure 3: eVTOL certification for take-off profiles and trajectory with take-off volume by EASA.

Most existing performance calculations for eVTOL aircraft have focused on only the two main segments: Hover and Cruise. For the cruise segment, where the flight velocity is mostly kept constant, analytical models typical use airplane derived formulas with steady level assumptions, while for the hover segment, where the aircraft is translating in the vertical axis, models typical use helicopter derived formula for each flight condition. Combining both models directly neglects the transition segment, as in transition the eVTOL aircraft experiences a transient and dynamic behaviour. The different flight segments for an eVTOL aircraft are shown in Figure 5, and the transition segments are highlighted in the orange boxes.

One notable study by Lovering, who analysed the performance of a tiltwing eVTOL aircraft modelled after Vahana [2]. Their study focuses on evaluating the direct operating cost based on the performance and operation requirements of a tiltwing eVTOL aircraft. An array of models was implemented to consider different aspects such as cost, structure, and mass. It is however, lacking in the modelling of the transition phase of an eVTOL whereby their models only consider the hover and cruise segments with their study being limited to a tiltwing configuration, thereby limiting the comparison with other eVTOL configurations.

Subsequently, another study by Johnson et al. [3] who compared different eVTOL configuration such as a quadrotor, tiltwing and a side-by-side helicopter. Their analysis was ran using NDARC with a dedicated focus on evaluating the performance of the hybrid and electric propulsion system. Besides Johnson et al., in a paper by Shawn et al. [4], different eVTOL configuration such as Lift + Cruise, Tiltrotor and Lift + Tilt have been modelled and compared. By modelling different configuration of eVTOL aircraft, both papers presented detailed comparisons of the characterisation of each configuration. However, like Lovering, the transition phase was the not carefully considered for each aircraft. In Johnson et al, it also highlighted that future work on the mission profile for the aircraft should be further investigated and refined.

Shamsheer [5] suggested a method to model the full flight regime of a tiltwing eVTOL configuration. In the study, the transition regime is being modelled for each individual time step. Moreover, the study covered the stall modelling for the tiltwing aircraft, highlighting that the aircraft might operate pass the stall region during the transition phase. However, the scope is limited to a tiltwing aircraft, neglecting other possible configurations such as Tiltrotors and Lift + Cruise. Nevertheless, their model was able to determine the power requirements for a given trajectory for a tiltwing aircraft.

Alternatively, Senkans et al. [6] also offers a different approach to model the transition segment. In their paper, they broke down the transition modelling into different segments, with specific requirements for each segment. Allowing for a more realistic and controlled trajectory to be modelled for a typical transition flight that comprises of different individual segments with different flight conditions. However, their trajectory model lacked the flexibility as it is restricted to using a constant acceleration and with power requirements being derived using simple momentum theory, that might not be fully representative of the dynamic transition regime with non-uniform inflows, thereby neglecting other power losses that a rotorcraft may incur.

In this research paper, our goal is to develop a complete transition model for a tiltrotor configuration, which will be also applicable for the other types of eVTOL configurations, with the intent to compare the different power requirement of various eVTOL aircraft configuration during the transition segment. This enables the estimation of the power and energy requirement, allowing for the appropriate sizing of the motors and battery systems. Thus, the intention behind our model starts from the basis that the power requirement is the main output of interest. The forces and the kinematic models are subsequently developed accordingly. The power model for our desired output will be discussed first, followed by the force and kinematic models. This is reflective of the thought process behind our modelling framework, basing off the approach using first principles.

2. TRANSITION MODEL

The eVTOL aircraft transition trajectory model consists of several modules to capture the different aspects of the transition flight phase of an eVTOL aircraft. These modules are developed in MATLAB in modular components, such that they are applicable to different types of eVTOL aircraft studies. A brief outline of the modelling framework and connections between the various modules are shown in Figure 4. It consists of four main modules: (1) power required, (2) trim force and moment, (3) kinematic and trajectory, and (4) aerodynamics. The aerodynamics module was based on previous work conducted [4], which was improved and implemented for a more comprehensive analysis.

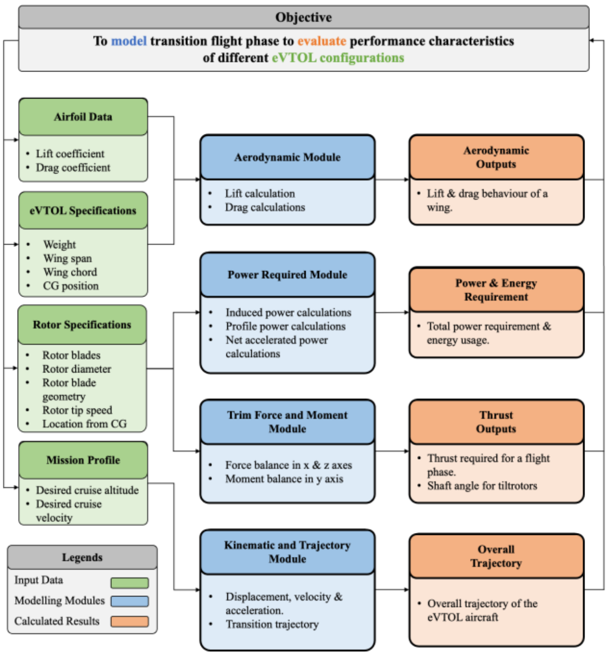

Figure 4: eVTOL Analysis framework

2.1 eVTOL Mission Profile

Main Mission Profile

For an eVTOL aircraft, Uber Elevate [7] has defined a few mission requirements that an eVTOL aircraft should consist of. As such a general mission profile for an eVTOL aircraft based on the different flight phases is shown in Figure 5.

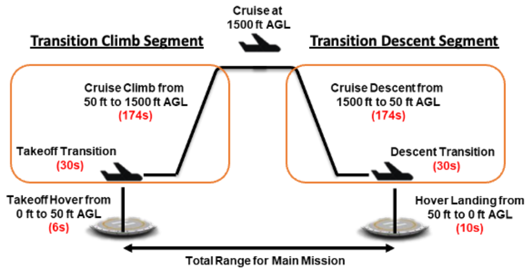

Figure 5: Main mission profile for an eVTOL aircraft.

Reserve Mission Profile

Similar to conventional aircraft such as transport aircraft and helicopters, an eVTOL aircraft must be able to perform a reserve mission in the event of unforeseen circumstances. In this case, the reserve mission will be set to cover 10% of the range covered by the main mission. The flight phases of a reserve mission profile are similar to the main mission, but flown at a low altitude, as shown in Figure 6.

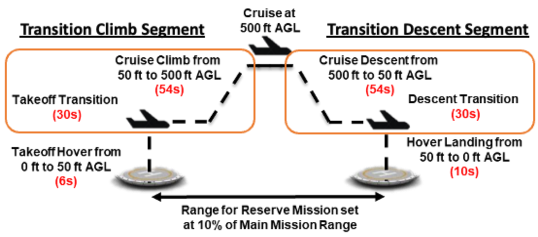

Figure 6: Reserve mission profile for an eVTOL aircraft.

The main and reserved mission comprises of different flight phases, that are constrained by the bounding condition during each phase of the flight. which is summarized in Table 1.

Table 1: Bounding condition for each flight segment.

Flight Segments	Main Mission		Reserve Mission	
	Altitude (m)	Time taken (s)	Altitude (m)	Time taken (s)
Takeoff Hover	15.24	6	15.24	6
Takeoff Transition	15.24	30	15.24	30
Cruise Climb	457.2	174	152.4	54
Cruise	457.2	TBD	152.4	TBD
Cruise Descent	15.24	174	15.24	54
Descent Transition	15.24	30	15.24	30
Hover Descent	0	10	0	10

In this paper, the takeoff transition and cruise climb are consolidated into the transition climb phase, while the cruise descent and descent transition are consolidated into the transition descent for both the main mission profile and reserve mission profile as shown in Figure 5 and in Figure 6 respectively.

2.2 Power Required Model

The power required model is modelled after the well-established Blade Element Momentum Theory (BEMT) from Helicopter Theory [8]. In BEMT, the Blade Element Method is the combination with Momentum Theory to derived induced power for each blade element across the span of the rotor blade, while capturing profile power. The Blade Element Method accounts for the blade properties, such as: the number of blades, the rotor tip speed, the drag coefficient of the blade. The Momentum theory, also known as Actuator Disk theory, determines the inflow of the rotors. Moreover, BEMT is also expanded to include the motion power of the aircraft to account for the aircraft manoeuvres during the transition flight phase. The total power is the summation of all the individuals power components. However, there are some limitations and assumptions made when using BEMT as shown in Table 2.

Table 2: List of assumptions.

Parameters Affected	Assumption	Assumed Values
Rotor Tip Speed	Constant speed	183 m/s
Rotor Blade Drag Coefficient	Constant value	0.012
Non-uniform Inflow Factor	Correction factor	9%
Tip Losses Factor	Correction factor	3%
Swirl Losses Factor	Correction factor	3%
Oswald Efficiency	Constant value	0.75
Electrical Efficiency	Constant value	0.9
Propulsive Efficiency	Constant value	0.85

As there are many different eVTOL configurations, their rotor blade design and properties will differ between these configurations. With the intent of generalizing the applicability of BEMT for different eVTOL aircraft analysis, this model assumes a uniform untwisted rectangular blade in the blade element calculations. Despite this assumption, it is still beneficial to use BEMT compared to momentum theory. With BEMT, it enables better accountability of the power requirements for an eVTOL aircraft rotor system, which may comprise of rotors of different dimensions, number of rotor blades or different profile, thereby increasing the fidelity of the power calculations. In this paper, BEMT is used to calculate the power requirements for both the vertical and horizontal propulsors. In the case of a rotor component, the vertical thrust is determined by the distributed weight of the aircraft; while the propeller component, the horizontal thrust is determined by the drag generated by the eVTOL aircraft.

The total power and the summation of all the power required components can also be expressed as a normalized value as shown in Equation (1) and (2). It should be noted that the parasite power is not being accounted in the power required module. The parasite power in typical helicopter theory is used to account for power required to overcome the overall drag of the aircraft. However, in this paper, the overall drag of the aircraft is accounted for as a cumulative drag coefficient using a component build-up method which is used to determine the total aircraft drag shown in Equation (15). To prevent double counting, the parasite power is omitted in the BEMT power calculation.

$$P_{req} = P_{induced} + P_{profile} + P_{net} \tag{1}$$

The normalization of power required P_{req} comprises of the area of the rotor disk πR^2, the density ρ and the rotor tip speed ΩR as shown in Equation (2),

$$C_P = C_{P_{induced}} + C_{P_{profile}} + C_{P_{net}} \quad \text{where } C_P = \frac{P_{req}}{\pi R^2 \rho (\Omega R)^3} \tag{2}$$

The normalized induced power in Equation (3), accounts for non-uniform inflow distribution and tip losses, an empirical correction factor, κ is used to formulate the induced power. A value of 1.15 was set for the correction factor, κ, with the breakdown of the correction factor being shown in Table 2. As normalized values are used for the velocity component, which in this case is the inflow ratio λ and the advance ratio μ, the induced power and thrust that generated is also normalized.

$$C_{P_{induced}} = \kappa \frac{C_T^2}{2\sqrt{\lambda^2 + \mu^2}} \tag{3}$$

The normalization of thrust, C_T in Equation (4), comprises of the area of the rotor disk, πR^2, the density, ρ and the tip velocity, ΩR.

$$C_T = \frac{T}{\pi R^2 \rho (\Omega R)^2} \tag{4}$$

The normalized profile power in Equation (5) is modified to account for the radial flow and reversed flow effects. To account for the normalized profile power, the rotor solidity, σ and blade airfoil drag coefficient, C_{d_0} is considered. Rotor solidity, σ is given to be the ratio of the area of the rotor blades to the area of the rotor disk.

$$C_{P_{profile}} = \frac{\sigma C_{d_0}}{8}(1 + 4.6\mu^2) \tag{5}$$

To account for the rotor solidity, the number of rotors, N, the chord length of the rotor blade, c and the radius of the rotor, R is accounted for as shown in Equation (6).

$$\sigma = \frac{NcR}{\pi R^2} \tag{6}$$

The normalized net power in Equation (7) for the unsteady motions of the aircraft is formulated similarly to the induced power. These motions include accelerated climb, descent and other unsteady behaviour during the aircraft flight phase.

$$C_{P_{net}} = \frac{T}{\pi R^2 \rho (\Omega R)^2} \times \frac{V_{net}}{\Omega R} = C_T \lambda_{net} \quad (7)$$

2.3 Trim Force and Moment Model

Aircraft Reference Coordinate System

One of the main components that is required for power calculation, as seen in Figure 4, is the thrust force generated by each rotor or propeller. During the transition segment, the thrust force is constantly changing, depending on the flight condition that the aircraft is in at any given time. Moreover, different eVTOL aircraft configuration has different rotor layouts and positions, affecting how the thrust force is being distributed along the entire rotor system.

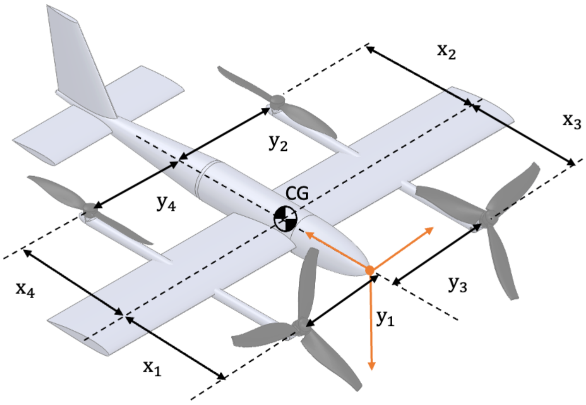

Figure 7: Rotor location system from CG on the aircraft.

By generalizing the rotor configuration using a defined coordinate system with the specified CG of the eVTOL aircraft, it allows different rotor layouts to be studied. The general coordinate system is derived with respect to the nose of the aircraft, as shown in Figure 7. The sign convention for the general coordinate system is as shown, as this is used to derive the sign direction of the loads during the calculation of trimmed forces and moments.

Aircraft Equation of Motion

With the general coordinate system for the location of rotors and CG location, the thrust and moment of each rotor about the CG location can be calculated. For the individual force balance for each of the axis are as shown in Equation (8):

$$F_x = \sum T_{x_{rotor_i}}, F_y = \sum T_{y_{rotor_i}}, F_z = \sum T_{z_{rotor_i}} \quad (8)$$

where $T_{()_{rotor_i}}$ is the thrust in each axis and i refers to the index of the rotor.

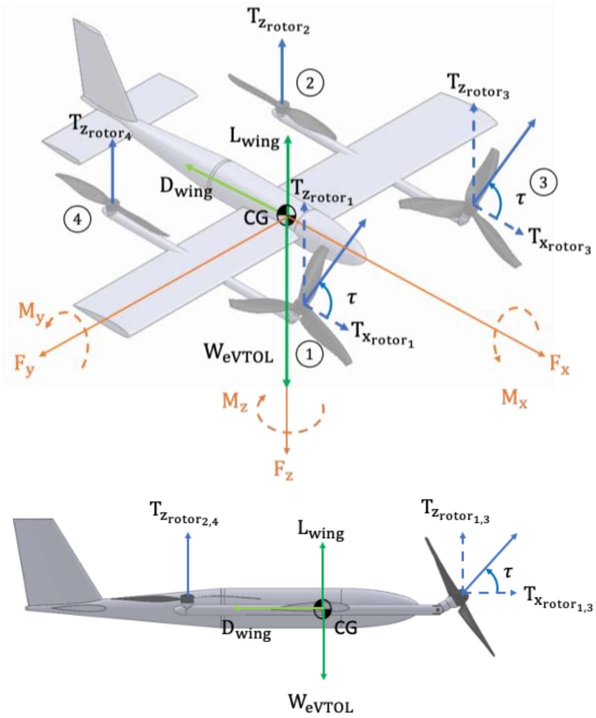

Figure 8: Free body diagram & modelling diagram.

The moment balance about the CG location is calculated using the matrix in Equation (9). In this study, symmetry is applied along the X-Z plane without any unbalanced forces acting along the y-axis whereby $F_y = \sum T_{y_{rotor}} = 0$.

$$\begin{bmatrix} M_{x_i} \\ M_{y_i} \\ M_{z_i} \end{bmatrix} = \begin{bmatrix} T_{x_{rotor_i}} \\ T_{y_{rotor_i}} \\ T_{z_{rotor_i}} \end{bmatrix} \times \begin{bmatrix} x_i \\ y_i \\ z_i \end{bmatrix} \quad (9)$$

where $x_i = X_{CG} - X_{rotor}$,
$y_i = Y_{CG} - Y_{rotor}$,
$z_i = Z_{CG} - Z_{rotor}$

Besides the rotor forces and moments, the aerodynamic forces and moments acting on the wing surfaces is accounted for by using 2D airfoil theory with an airfoil element along the wingspan.

The velocity components and their respective angles are shown in Figure 9, to determine the aerodynamic forces acting on the airfoil. The airfoil has a pitch angle, θ which is measured from the inertial frame axis to the body frame axis of the airfoil. As the aircraft translates horizontally and vertically, this induces an additional velocity component acting on the airfoil from the velocity component in the horizontal and vertical axis, V_{∞_x} and V_{∞_z} respectively.

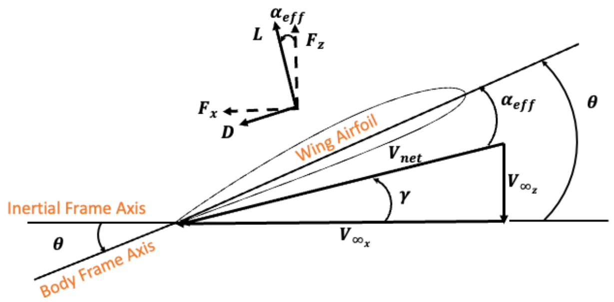

Figure 9: Velocity components and forces on a wing airfoil

This results in a resultant velocity component, V_{net} with an induced angle, γ which is known as the aircraft climb angle, that is calculated using Equation (10). This leads the airfoil to be at an effective angle of attack, whereby the effective angle of attack α_{eff} is the difference between pitch angle θ and climb angle γ, which is calculated using Equation (11). The effective angle of attack is defined as α_{eff} and is used to calculate the lift and the drag forces.

$$\gamma = \tan^{-1}\frac{V_{\infty_z}}{V_{\infty_x}} \tag{10}$$

$$\alpha_{eff} = \theta - \gamma \tag{11}$$

$$\mathrm{V_{net}} = \sqrt{V_z^2 + V_x^2} \tag{12}$$

The lift and drag forces are calculated according to both Equation (13) and (14) respectively. Both the lift and drag forces are functions of the resultant velocity, V_{net}, density, ρ, wing area, S and lift coefficient, C_L and drag coefficient, C_D. However, as the effective angle of attack α_{eff} changes depending on the pitch angle θ and climb angle γ, this affects the lift coefficient C_L and drag coefficient C_D which are functions of the effective angle of attack. The drag coefficient C_D is made up of two components: parasite drag coefficient C_{D_0} and induced drag coefficient C_{D_i} as shown in Equation (15).

$$L_{wing} = \frac{1}{2}\rho V_{net}^2 S C_{L_\alpha}\alpha_{eff} \tag{13}$$

$$D_{wing} = \frac{1}{2}\rho V_{net}^2 S(C_{D_\alpha}\alpha_{eff} + C_{D_{Fuselage}}) \tag{14}$$

In this case, induced drag coefficient is a function of the aspect ratio, AR and Oswald efficiency, e, which is taken to be 0.75. Experimental data is used to account for the effect of angle of attack over a wide range on the lift and drag coefficient. From Figure 10, it shows the lift coefficient C_L and drag coefficient C_D for angle of attack α between 0° to 360°. For this study, extrapolated C_L and C_D values are used for the range of angle of attack α between $-90°$ to $+90°$.

$$\sum C_{D_\alpha} = C_{D_0} + C_{D_i} = C_{D_0} + k(C_{L_\alpha}\alpha_{eff})^2 \tag{15}$$

where $k = \frac{1}{\pi e AR}$

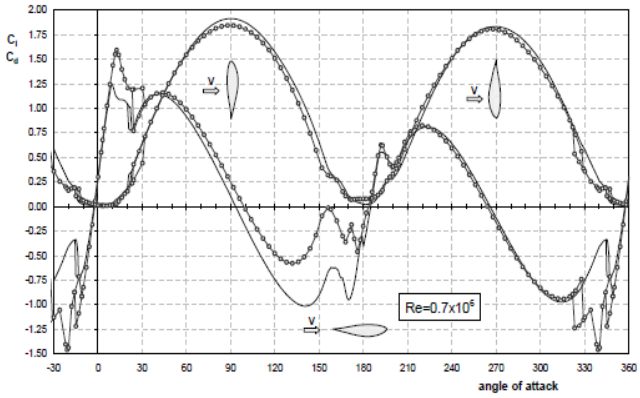

Figure 10: DU 96-W-180 Airfoil Lift and Drag coefficients [9].

2.4 Kinematic and Trajectory Model

General Kinematic Equations for Modelling

The transition segment of an eVTOL aircraft is both dynamic and transient in nature, as compared to cruise or hover segments that are evaluated in steady conditions. In transition, the velocities and the accelerations are constantly changing in every time frame. Thus, the equation of motion derived from the trim matrix alone is incomplete without a kinematic model to define the trajectory of the aircraft. Using Newton's second law shown in Equation (16), the force is a function of acceleration for a given mass about each axis, thus, the acceleration component is required to determine the instantaneous forces and moments to balance the eVTOL aircraft.

$$\sum \vec{F_i} = m_{eVTOL}\vec{a_i} \tag{16}$$

where $\sum \vec{F_i}$ and $\vec{a_i}$ is the resultant force vector and acceleration vector in each axis.

In the vertical axis, the aircraft starts at a vertical displacement S_z for the given trajectory, representing the flight altitude. The vertical velocity V_z and vertical acceleration a_z are determined using Equations (17).

$$\therefore V_z = \frac{dS_z}{dt}, \qquad \therefore a_z = \frac{dV_z}{dt} \tag{17}$$

Similarly, in the horizontal axis, the aircraft starts with a horizontal velocity V_x for a given trajectory, representing the flight velocity. the horizontal acceleration a_x and horizontal displacement S_z are determined using Equations (18).

$$\therefore a_x = \frac{dV_x}{dt}, \qquad S_x = \int V_x\,dt \tag{18}$$

Trajectory Parabolic Function

A defined function is used to represent the aircraft trajectory with the desired altitude and velocity. A simple curve parabolic function is used to define the transitional trajectory from stationary hover to cruise, representing the trajectory of the transition phase that includes the vertical climb portion to the desired altitude and horizontal acceleration to the cruise speed. This is modelled using the function as shown in Figure 11.

The parabolic function $f(t)$, as shown in Equation (19), is given to be the vertical translation S_z or the horizontal velocity V_x, that are a function of time t. The coefficient a and b are constant values adjusted to model the different transition parameters. For our study, we chose to change the coefficient a as it affects the gradient of the curve and results in greater variations than coefficient b, allowing for different trajectory to be modelled. The value of coefficient *b* is kept constant at 3.

$$f(t) = 1 - e^{-\left(\frac{t}{a}\right)^b} \quad (19)$$

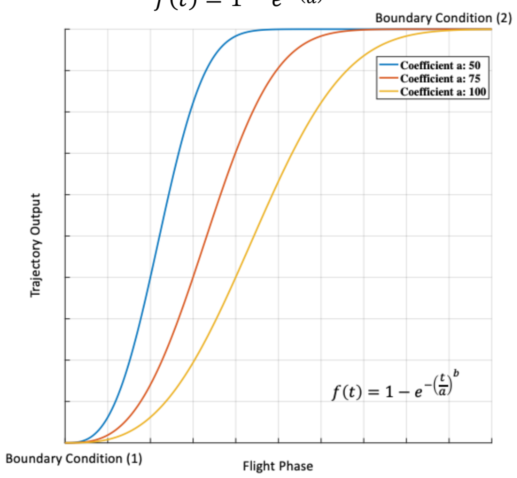

Figure 11: Trajectory function used to model the trajectory for vertical translation and horizontal velocity.

Three different modelling studies was conducted using the various presented modelling modules. Firstly, the study of the ratio of lift contribution by wing for various tilt angles of a tiltrotor representing different types of eVTOL aircraft configuration. Secondly, the study of transition climb and descent based on the eVTOL aircraft trajectory. Finally, the performance comparison of different eVTOL aircraft configurations consisting of a Lift + Cruise, Tiltrotor and Lift + Tiltrotor. The purpose of these studies is to investigate and evaluate the performance of eVTOL aircraft based on different conditions and trajectories as well as their different aircraft configurations.

3. RESULTS AND DISCUSSIONS

3.1 Effect of Tilt Angle on Lift Contribution

In this section, a study on the generic eVTOL aircraft with tilting front rotors was investigated to determine the effects of both the tilt shaft angle and the flight velocity on the ratio of lift contribution from the wing. The effect of both parameters allows for the understanding of the flight characteristics of an eVTOL aircraft with tilting front rotors during transitional flight. The assumption made in this analysis is that the aircraft is constantly in steady level horizontal flight, without exhibiting any climb or altitude change, thereby having no vertical velocity and acceleration components being considered. Additional propwash effect will be taken as a secondary effect and is not included in this analysis. Besides that, lift from the tail is assumed to be very small due to the large tail moment arm, hence, the lift generated by the tail is considered to be negligible and majority of the lift is being generated by the wing.

Table 3. Test cases for different tilt angle

Case	Shaft Angle τ	Modelling Characteristics	
1	90°	Multicopter	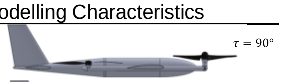
2	60°	Tiltrotor	
3	30°	Tiltrotor	
4	0°	Airplane	

The test cases modelled are according to a fixed shaft angle for the tiltable front rotors as shown in Table 3. The cases modelled are: (1) $\tau = 90°$ which has the model behave similar to a multicopter, (2) $\tau = 60°$ and (3) $\tau = 30°$ which have the model behave similar to a tiltrotor, and lastly (4) $\tau = 0°$ which has the model behave similar to an airplane.

The results on how the tilt angle affects the lift contribution from the wing is shown and discussed accordingly for each shaft angle. The contribution of lift is defined by the ratio of lift contribution as shown in Equation (20).

$$\text{Ratio of lift contribution} = \frac{\mathrm{L_{wing}}}{\mathrm{W_{eVTOL}}} \quad (20)$$

For this study, the test model of interest is the generic eVTOL aircraft model with tilting front rotors and the inputs for the analysis are shown in Table 4. The inputs are based on values for a typical full-size passenger carrying eVTOL aircraft with a mass of 3175kg.

Table 4. Input values for generic eVTOL aircraft model

Parameters	Generic eVTOL Aircraft Model
m_{eVTOL} (kg)	3175
Wing Area	26.76 m^2
Wing Aspect Ratio	8.41
Oswald Efficiency Number	0.75
Rotor Diameter	3.91 m
Solidity	0.115
C_{d_0} for Rotor Blade	0.012
Rotor tip speed (m/s)	183
$C_{d_{fuselage}}$	0.02
Max Rotor Thrust (N)	20,000

3.1.1 Study of Ratio of Lift Contribution by Wing

The ratio of lift contribution by the wing is seen in Figure 12, whereby the blue line indicates $\tau = 0°$ for an airplane configuration, while the orange and yellow line indicates $\tau = 30°$ and $\tau = 60°$ for a tiltrotor configuration, and the purple line indicate $\tau = 90°$ for a multicopter configuration.

Initially, up to $70 \mathrm{m/s}$, the ratio of lift increases along a common curve, as seen in Figure 12. This line follows the lift curve slope, which is govern by the lift equation as shown in Equation (13).

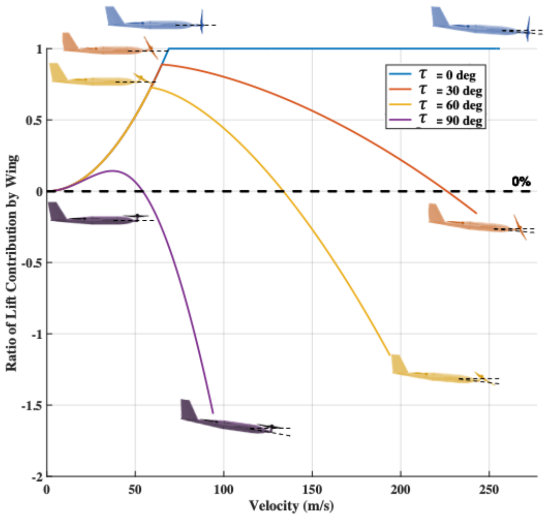

Figure 12: Ratio of lift contribution by wing against velocity for different shaft angle

As for the pitch angle of the eVTOL aircraft as shown in Figure 13. The negative pitch plot shows the angle required for the aircraft to travel at a given horizontal forward velocity.

The results presented are used to evaluate the behaviour and the characteristics of the different configuration of eVTOL aircraft and to understand the effects of the tilt shaft angle and horizontal velocity on the contribution of lift from the wing of an eVTOL aircraft. The following sections details the effect of having the shaft angle, τ for each case.

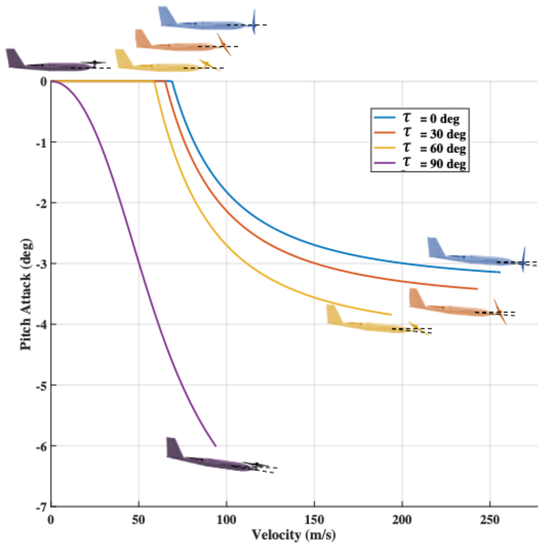

Figure 13: Pitch angle against velocity

Shaft Tilt Angle at $90°$

The ratio of lift contribution by wing for the shaft tilt angle at $90°$ increases and then decrease into the negative region with increasing velocity, as shown in Figure 12.

At $\tau = 90°$, the aircraft behaves similar to a multicopter, whereby the aircraft would initially be in a steady hover. At this shaft angle, the thrust produced by the front and back rotors must equal to the weight of the eVTOL aircraft, as shown in Figure 14, and formulated in Equation (21): with the summation of force from the rotors being equal to the weight of the eVTOL aircraft. In this initial state, the eVTOL aircraft is stationary.

$$\Sigma T_{z_{rotor_i}} = W_{eVTOL} \tag{21}$$

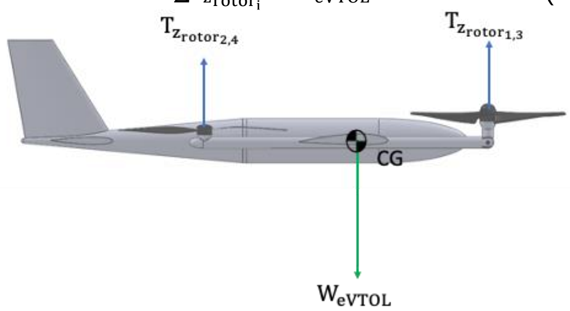

Figure 14: Forces in the hover state for $\tau = 0°$.

For a typical multicopter to gain horizontal velocity, it is achieved by pitching the aircraft forward to provide a horizontal force and velocity as shown in Figure 15.

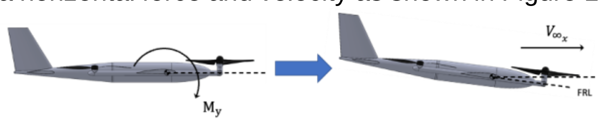

Figure 15: Horizontal motion of a multicopter.

By pitching forward, the aircraft then gains forward velocity, thus having the wing surfaces to generate both lift and drag forces as shown in Figure 16, with the forces acting on the aircraft during horizontal motion.

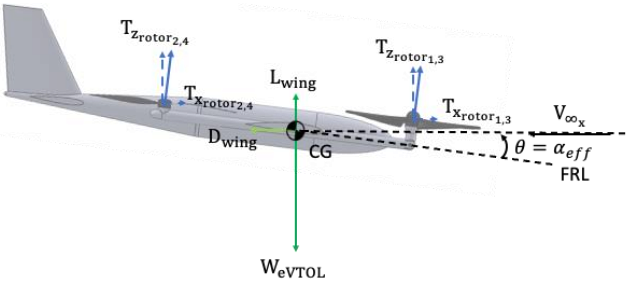

Figure 16: Forces in horizontal motion for $\tau = 0°$.

The summation of forces in the vertical axis from Equation (22), comprises of the thrust from the rotors and the lift generated by the wing to be equal to the weight of the aircraft. While the summation of forces in the horizontal axis from Equation (23), comprises of the horizontal thrust forces of the rotors being equal to the drag of the aircraft. Finally, the summation of all moments about the CG from Equation (24), is due to the moment arm of the thrust of the rotors that must be equated to zero. The aircraft is then able to achieve a steady level forward flight by satisfying all the Equations (22) to (24).

$$\sum T_{z_{\text{rotor}_i}} + L_{\text{Wing}} = W_{\text{eVTOL}} \quad (22)$$

$$\sum T_{x_{\text{rotor}_i}} = D_{\text{wing}} \quad (23)$$

$$\sum T_{z_{\text{rotor}_i}} \times \text{Distance from CG} = 0 \quad (24)$$

As the aircraft continues to pitch further forward to gain greater horizontal velocity, the airfoil of the wing experiences a negative angle of attack as shown in Figure 17. An aircraft at a negative angle of attack can continue to have a positive lift coefficient, due to a positive camber on the airfoil as seen in both Figure 16 and Figure 10. However, the lift coefficient becomes negative when the angle of attack is at large negative angle, which occurs as the aircraft pitches further forward to gain higher horizontal velocities. As such, this induces a negative angle of attack on the airfoil, thereby resulting in negative lift and a negative wing lift contribution ratio.

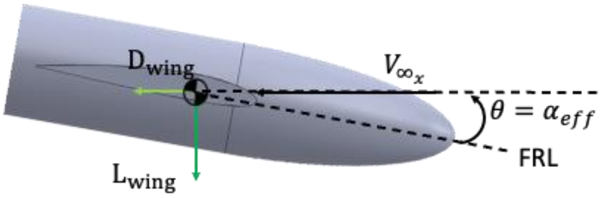

Figure 17: Negative lift cause by pitch angle.

The pitch angle for $\tau = 0°$ is shown in Figure 13, where the aircraft pitch angle increases drastically with greater horizontal velocity. This highlights that the aircraft at $\tau = 0°$ behaves similarly to a multicopter configuration is unable to achieve high forward velocity, as the rotors are thrust limited to counteract the negative lift generation by the wing, thus preventing the aircraft to attain higher speed. Therefore, an eVTOL aircraft or a multicopter configuration with wing surfaces should be designed with an angle of incidence on the wing to prevent a large induced negative angle of attack on the wing when the eVTOL aircraft travels horizontally.

Shaft Tilt Angle at $60°$ and $30°$

The ratio of lift contribution by wing for the shaft tilt angle at $60°$ and $30°$ increases along a similar slope, subsequently, the lift contribution decreases into the negative region as shown in Figure 12,

At $\tau = 60°$ and $30°$, the aircraft behaves similar to a tiltrotor aircraft, where the aircraft is no longer like a multicopter, the aircraft is able to gain some horizontal velocity without having to pitch forward. This is because the front tilting rotors can be tilted at an angle to provide the forces required. The thrust force produced by the front tilting rotors results in a horizontal component to allow the aircraft to gain horizontal velocity without requiring forward pitching.

Hence, at $\tau = 60°$ and $30°$, the force and moment balance about the CG must continue to satisfy the Equation (22) to (24) in order to maintain steady level forward flight as shown in Figure 18 and Figure 19.

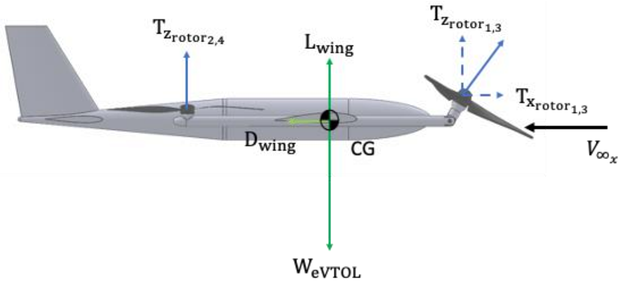

Figure 18: Forces of a tilt configuration with $\tau = 60°$ initially.

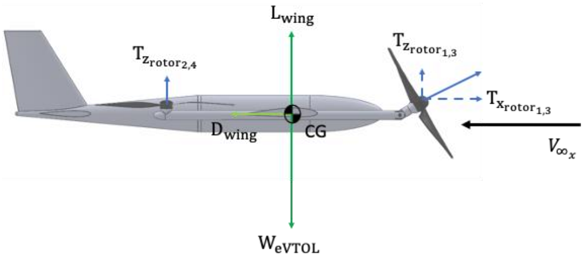

Figure 19: Forces of a tilt configuration with $\tau = 30°$ initially.

However, for an aircraft with a fixed shaft angle, to gain increased horizontal velocity, the aircraft similarly has to pitch forward as shown in Figure 20. The behaviour is similar to when $\tau = 0°$ and the aircraft has to the pitch forward, as shown in Figure 15. The pitch angles for $\tau = 60°$ and $30°$ is shown in Figure 13 where the aircraft pitches forward more at higher forward velocities.

By pitching forward, the airfoil of the wing on the aircraft experiences a negative angle of attack as shown in Figure 17. Positive lift coefficient can be maintained at lower forward velocities, as shown in Figure 20, until when the angle of attack becomes too negative, resulting in the generation of negative lift.

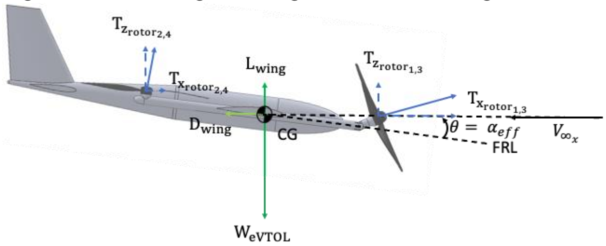

Figure 20: Forces of a tilt configuration with $\tau = 30°$ to gain more horizontal velocity.

Comparing between both shaft angles from Figure 12, an aircraft with shaft angle of $30°$ can reach higher velocity than with a shaft angle of $60°$. This is because the tilted front rotors overcomes the drag force at higher speed, when tilted to a lower angle. As a result, for higher velocities, an aircraft with shaft angle of $30°$ is not required to pitch forward as much as an aircraft with shaft angle of $60°$ as shown in Figure 13.

Shaft Tilt Angle at 0°

The ratio of wing lift contribution for the shaft tilt angle at $0°$ increases along an identical lift curve slope until it reaches unity at the stall velocity as shown in Figure 12, and with the stall speed is being calculated using Equation (25). The lift contribution remains constant at all velocities as the lift is used to support the weight.

$$V_{stall} = \sqrt{\frac{2}{\rho}\frac{W}{S}\frac{1}{C_L}} \tag{25}$$

At $\tau = 0°$, the aircraft is able to fly similar to a conventional airplane, which is able to gain horizontal velocity without requiring any pitching forward motion as the front rotors are aligned parallel to the forward flight axis as shown in Figure 21. With $\tau = 0°$, the aircraft continues to satisfy the Equation (23), while the Equation (22) is modified to Equation (26), with the vertical forces being equated to only the wing lift.

$$L_{wing} = W_{eVTOL} \tag{26}$$

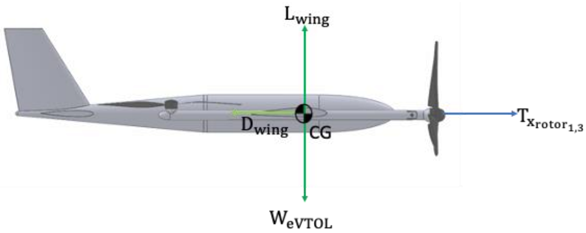

Figure 21: Forces of a tilt configuration with $\tau = 0°$

However, with the assumption of steady level flight, the aircraft with $\tau = 0°$ has to pitch forward slightly as shown in Figure 13 in order to prevent the eVTOL aircraft from climbing or ascending with exceed lift.

3.1.2 Comparison of Power Required

For each shaft tilt angle τ, the aircraft have different power requirements as shown in Figure 22. At $\tau = 90°$, the power required is the least as it is limited by its forward velocity. While at τ values of $60°$ and $30°$, the overall power required increases, due the higher achievable forward velocities. Finally, at $\tau = 0°$ the power required decreases significantly, as the fixed rear rotors are shut-off as shown in Figure 24.

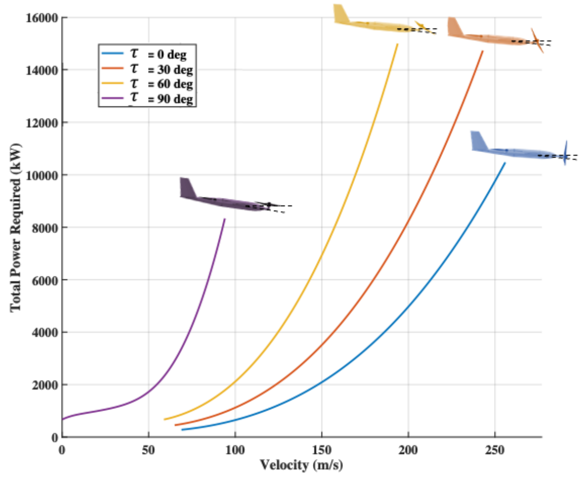

Figure 22: Total power against forward velocity

At $\tau = 90°$, the power required for both the front and back rotors is the same as shown in Figure 23 and Figure 24. This is expected as the front and back rotors are equally loaded. While for other shaft angles, for the same forward velocity, the power required for the front and rear rotors is reduced with a lower shaft angle. This is because the front rotors are less burdened as the weight of the eVTOL aircraft is supported by the wing surfaces. At $\tau = 0°$, the power for the stationary rear rotors is at a minimum as the weight is fully supported by the wings.

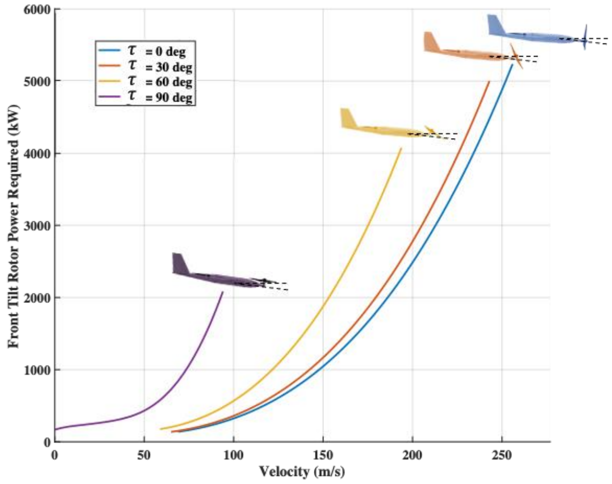

Figure 23: Front tiltrotor power against velocity

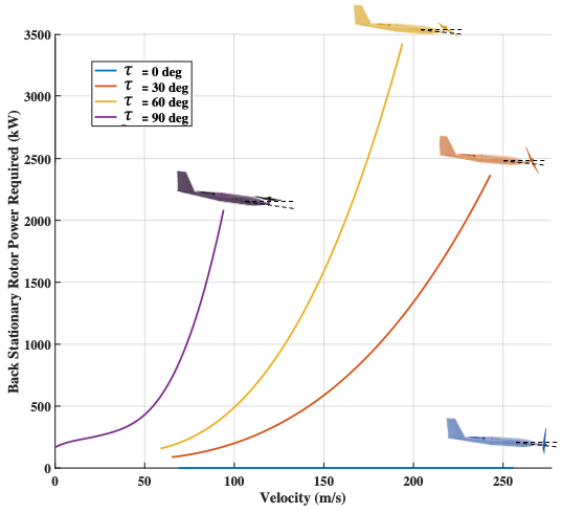

Figure 24: Back stationary rotor power against velocity

This study is important in showing the benefits of a tiltrotor aircraft. With a tiltrotor design, an eVTOL aircraft can gain horizontal velocity without having to pitch as much as an eVTOL aircraft with a multicopter configuration.

As a result, the lift contribution by the wing surface can remain positive for a wider range of velocities, allowing the forces supporting the aircraft weight to be transferred from the rotors to the highly efficient wing surfaces, hence allowing higher achievable velocities to be reached. The power required for tilting the rotor increases correspondingly to the change in shaft angle until the aircraft transition to a complete forward flight, thereby highlighting greater efficiency during high speed flight for the tiltrotor aircraft designs.

3.2 Effect of Transition Climb and Descent Trajectory

In the second study, the objective is to investigate the effect of the transition trajectory for the transition climb and descent segments in terms of the flight profile parameters as well as the power required to execute the transition manoeuvre. This involves the definition of the transition equations and kinematics that are used to represent the transition manoeuvre and the forces acting on the aircraft. The aircraft model used is the same generic eVTOL model as shown in Section 3.1. A moderate transition trajectory in the form of the trajectory function is used. The inputs for the trajectory function for altitude and velocity is given by Equation (27), and is shown in Table 5. With the typical cruising velocity for an eVTOL aircraft being between 69 m/s to 91 m/s [10, 11], a cruise velocity of 70 m/s is used for the analysis.

$$f(\mathrm{t}) = \mathrm{C}_1\left(1 - e^{-\left(\frac{t}{a}\right)^b}\right) \tag{27}$$

Table 5: Coefficients values for trajectory function.

Flight Phase	Parameters	C_1	a	b
Transition Climb	Altitude	460	100	3
	Velocity	70	100	3
Transition Descent (Vertical Landing)	Altitude	460	110	3
	Velocity	70	143	3
Transition Descent (Non-vertical Landing)	Altitude	460	-	-
	Velocity	70	-	-

Following the certification requirements [1], the transition climb trajectory follows a Vertical Take-off approach as shown in Figure 3. While the transition descent trajectory is broken up into two approaches namely: (1) vertical landing and (2) non-vertical landing as shown in Figure 34.

The defined trajectory function is used to determine the acceleration values for transition climb and the deceleration values for the vertical landing transition descent. While a linear trajectory function is used for the non-vertical landing transition descent, as some eVTOL configurations does not have a mechanism to decelerate the aircraft by using its rotor systems. Hence, a linear trajectory is defined for the non-vertical landing transitional descent that is used to model the transition descent flight phase within the main mission profile. In this study, both transition descent models are investigated.

3.2.1 Transition Climb

In this section, the modelling on a generic eVTOL aircraft for a transition climb is discussed. The assumption made for this study is that the aircraft is performing a level climb, in which the eVTOL aircraft does not pitch during this transition phase. Hence, the fuselage reference line is aligned with the horizon. The trajectory that is modelled is similar to the vertical take-off trajectory as shown in Figure 3. As such, there is a climb angle, measured from the horizon, that the eVTOL aircraft follows as shown in Figure 25.

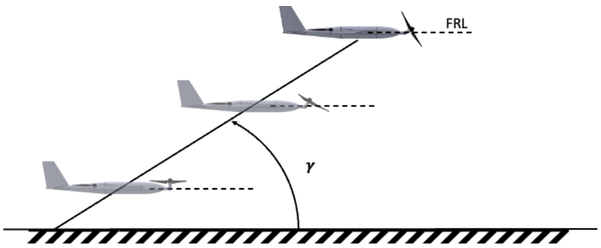

Figure 25: Measurement of climb angle with reference to the horizon

Transition Climb Equations

The equation of motion for the transition climb is derived for this study using the trim force and moment modelling equations. For transition climb, it is possible that an eVTOL aircraft is accelerating in both the horizontal or vertical directions simultaneously, which means that the eVTOL aircraft is flying in a dynamic state instead of a steady state along the x-axis and z-axis. Therefore, acceleration in both the horizontal and vertical direction must be accounted for.

Additionally, the forces must be in equilibrium for both the vertical and horizontal axis respectively, following Equations (28) and (29). In the case when there is negative lift, both Equations (28) and (29) can account for it. From Equation (30), the summation of all moments about the CG, due to the moment arm of the individual thrust of the rotors, must be zero to ensure that the aircraft is not pitching and the fuselage reference line is parallel to the horizon as shown in Figure 25. For this study, the lift from the tail is assumed to be very small and negligible.

$$\sum \mathrm{T}_{\mathrm{z}_{\mathrm{rotor}_i}} + \mathrm{L}_{\mathrm{wing}_z} - \mathrm{D}_{\mathrm{wing}_z} - \mathrm{W}_{\mathrm{eVTOL}} = \mathrm{m}_{\mathrm{eVTOL}} \times \mathrm{a}_z \quad (28)$$

$$\sum \mathrm{T}_{x_{\mathrm{rotor}_i}} - \mathrm{L}_{\mathrm{wing}_x} - \mathrm{D}_{\mathrm{wing}_x} = \mathrm{m}_{\mathrm{eVTOL}} \times \mathrm{a}_x \quad (29)$$

$$\sum \mathrm{T}_{\mathrm{z}_{\mathrm{rotor}_i}} \times \text{Distance from CG} = 0 \quad (30)$$

Transition Climb Kinematics

With the trajectory function being defined, the kinematics variables such as, distance, velocity and acceleration can be determined, as shown in Figure 26 for both the vertical and horizontal axis.

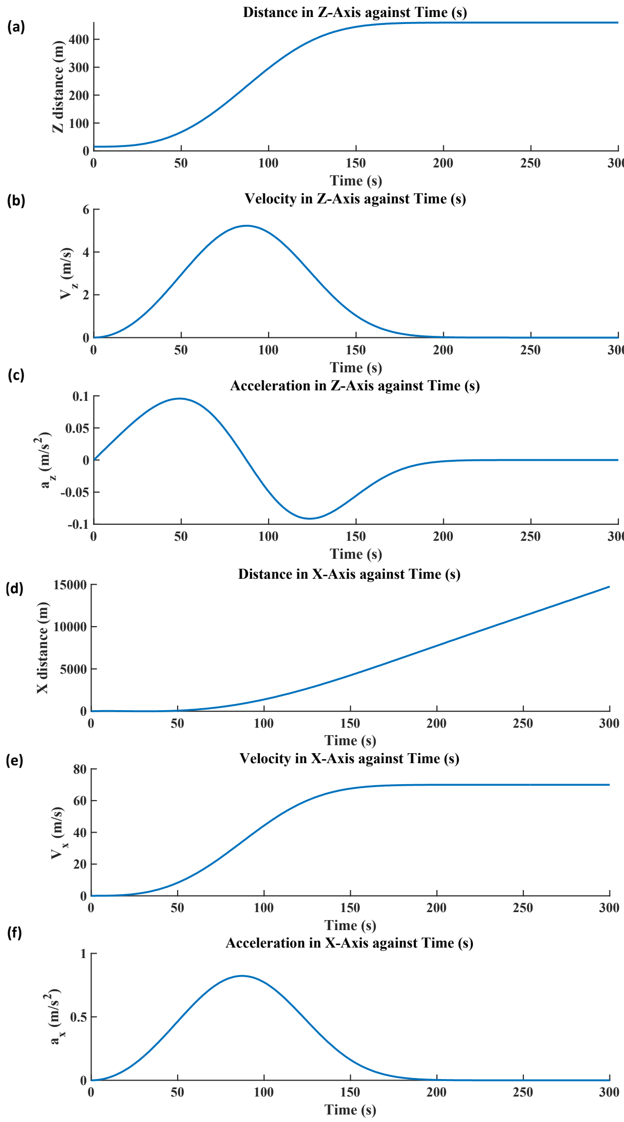

Figure 26: Transition climb results against time for: (a) vertical translation; (b) vertical velocity; (c) vertical acceleration; (d) horizontal translation; (e) horizontal velocity; (f) horizontal acceleration.

The climb angle and the overall trajectory is shown in Figure 27 (a) and (c) respectively. The eVTOL aircraft ascend at the start before translating horizontally shortly after, hence the climb angle starts from a large value during hover, and eventually decreasing to a smaller climb angle during cruise.

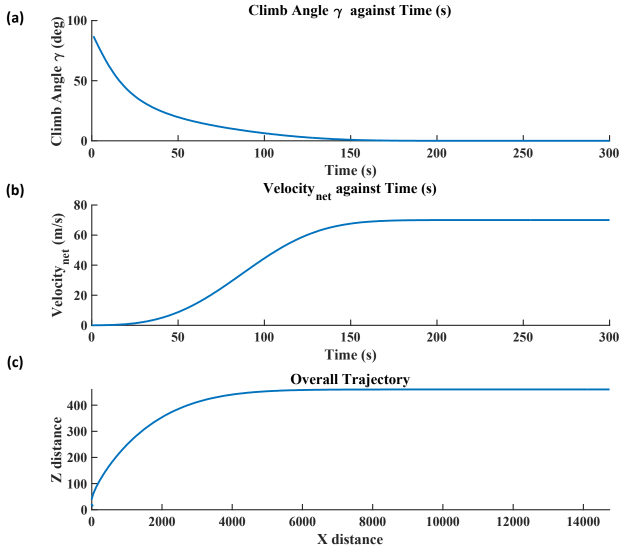

Figure 27: Transition climb results against time for: (a) climb angle; (b) resultant velocity; (c) overall trajectory.

Using the data from Figure 10, the lift and drag coefficient are matched against the climb angle of the eVTOL aircraft as shown in Figure 28.

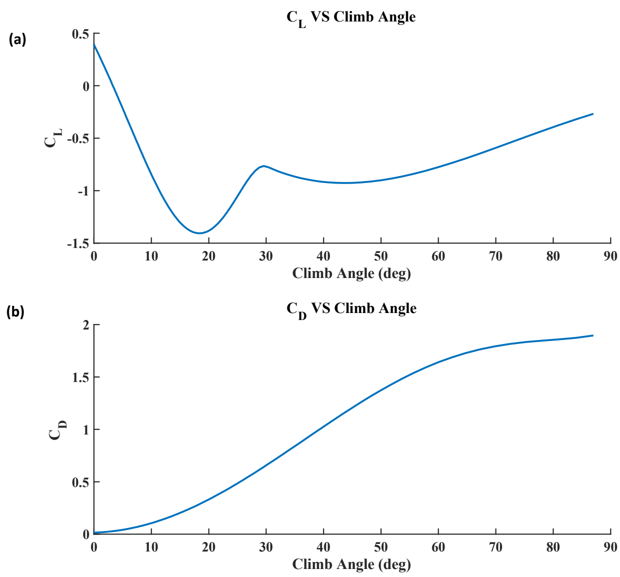

Figure 28: Transition climb results against climb angle for: (a) lift coefficient; (b) drag coefficient.

Transition Climb Forces

In a transition climb, the thrust required by the rotor in the vertical direction increases to support the increase in negative opposing force, which is made up of two individual components of: the lift and drag components in the vertical direction. From Figure 29 (b), the lift component is the major component, and the drag component is not a significant component in the vertical direction, due their lower order of magnitudes.

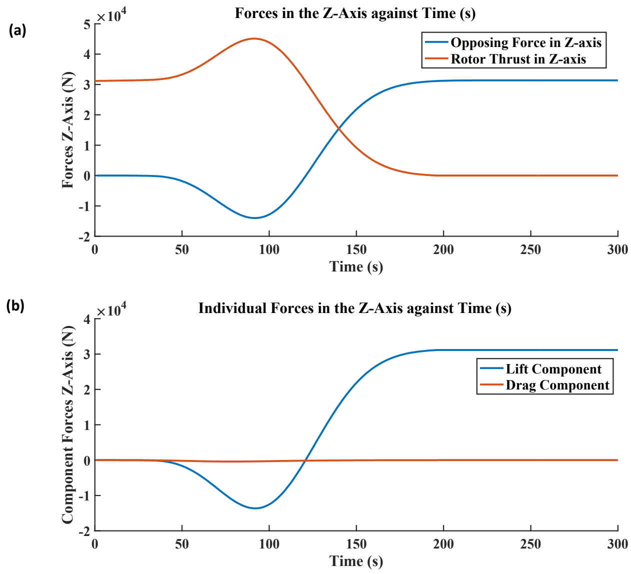

Figure 29: Transition climb results against time for: (a) vertical rotor thrust and opposing force; (b) vertical lift and drag components.

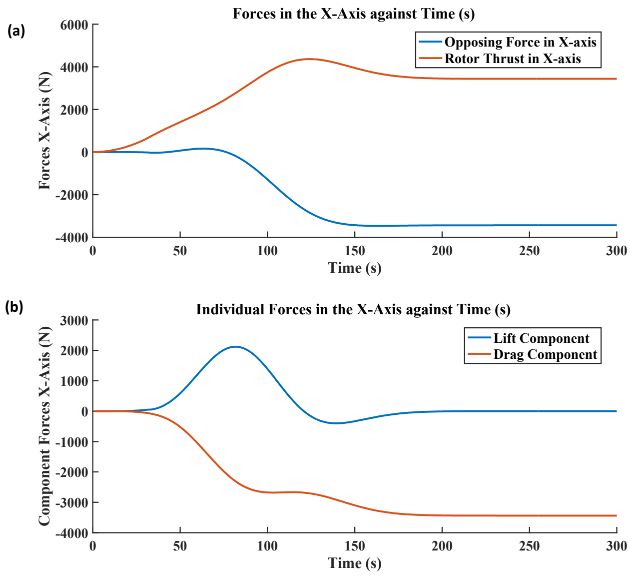

Figure 30: Transition climb results against time for: (a) horizontal rotor thrust and opposing force; (b) horizontal lift and drag components.

During transition climb, when the vertical velocity is larger than the horizontal velocity, a large climb angle to be induced along with a resultant velocity as shown in Figure 31 (a). The climb angle induces a negative effective angle of attack on the airfoil. This results in a negative lift generated in the wind reference frame. The result of the negative lift leads to the increase in negative opposing force. This negative lift burdens the rotors, as it is required to generate additional thrust to support the aircraft as shown in Figure 29 (a). Eventually, the climb angle reduces to a smaller value as shown in Figure 27 (a) for this trajectory.

At a small climb angle, the force and velocity components for the eVTOL aircraft are shown in Figure 31 (b). The lift and drag are generated due to the resultant velocity on the wing. At small climb angle, the induced negative angle of attack is small.

The lift coefficient is positive at small negative angle of attack, due to the positive chamber of the airfoil, as shown in Figure 10. Thus, the generation of positive lift from the smaller climb angle supports the weight of the eVTOL aircraft, and hence the thrust required from the rotors is reduced.

The thrust required by the rotors in the horizontal direction as shown in Figure 30 (a), is on an increasing trend due to the positive acceleration from Figure 27 (c). For the opposing horizontal forces, which comprises of the lift component and the drag component as shown in Figure 30 (b), the forces remain relatively constant initially; due to the cancelling effect of negative lift and negative drag component, and increases negatively to a constant negative value subsequently, due to the generation of positive lift.

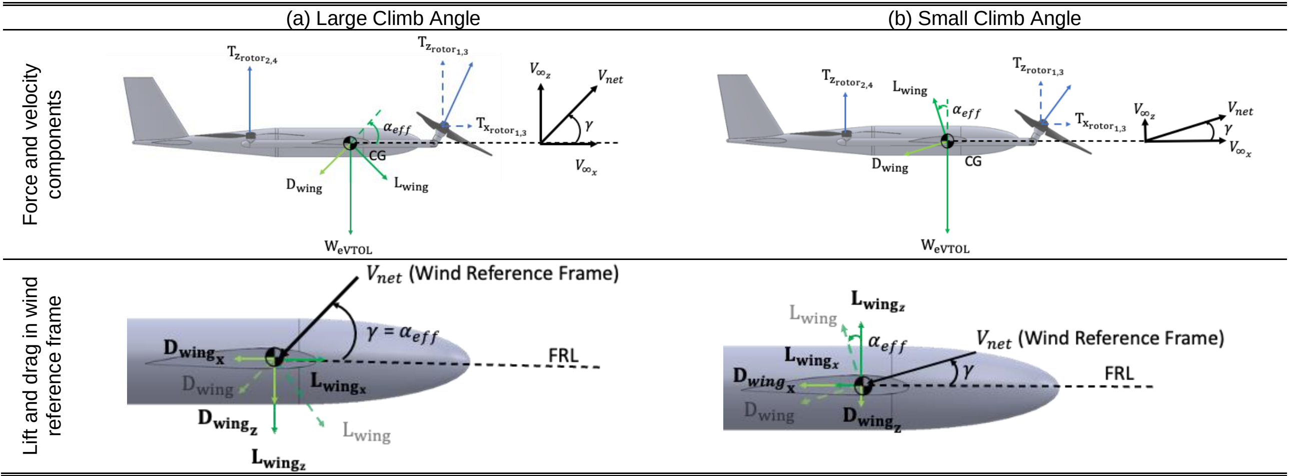

Figure 31: Forces on an eVTOL aircraft and velocity components for transition climb.

Transition Climb Power Required

The transition climb sees an increase in total power required as shown in Figure 32. The power required from the front tilting rotor plays the major role in the increase in total power as it is responsible to provide thrust in both the horizontal and vertical direction. The power required by the lift-rotor is to only provide the vertical thrust to support the eVTOL weight.

As the wing of the aircraft gains more horizontal velocity, positive lift is generated to support the weight of the eVTOL aircraft, reducing the burden on the rotors. This results in a decrease in the power requirement for the tiltrotor and lift-rotor.

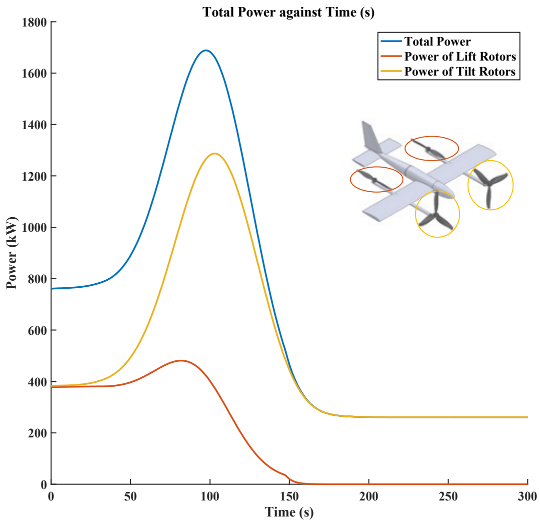

Figure 32:Transition climb - total power, power of lift-rotors and power of tit rotors against time.

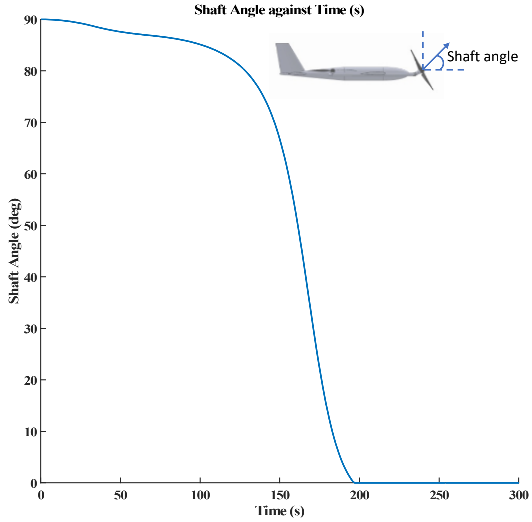

Figure 33: Transition climb - shaft angle of the front tiltable rotor against time.

Towards the end of the transition climb phase, the power required by the eVTOL aircraft is only from the tiltrotor, to overcome the drag of the aircraft hence total power curve coincide with the tiltrotor power curve as shown in Figure 32. The shaft angle of front tiltable rotor can also be calculated and the trend is shown in Figure 33.

Initially, the shaft angle decreases slightly to gain horizontal velocity as shown in Figure 33, which is also shown from the study in Section 3.1. During this period, the shaft angle is kept at an almost constant value, to provide sufficient horizontal and vertical forces for the eVTOL aircraft in transition climb. Ultimately, the wing surface of the eVTOL aircraft is able to generate sufficient lift to reduce the reliance on the tiltrotor for vertical thrust component. As such, the tiltrotor can tilt at a faster rate into a forward flight configuration to cruise at a lower power setting as shown in Figure 32.

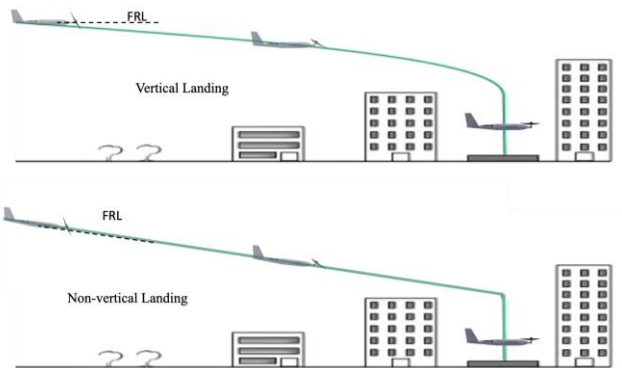

Figure 34: Transition descent vertical landing (top); transition descent non-vertical landing (bottom).

3.2.2 Transition Descent

For transition descent, there are two types of descent that can be modelled: (1) the first would be the opposite trajectory for transition climb representing a vertical landing and (2) a non-vertical landing sequence as shown in Figure 34.

For the vertical landing, the eVTOL aircraft performs a level descent, in which the fuselage reference line is parallel to the horizon as shown in Figure 35. For the non-vertical landing, the eVTOL aircraft performs a pitched descent, in which the fuselage reference line is no longer parallel to the horizon, and the pitch angle varies with the descent angle shown in Figure 34.

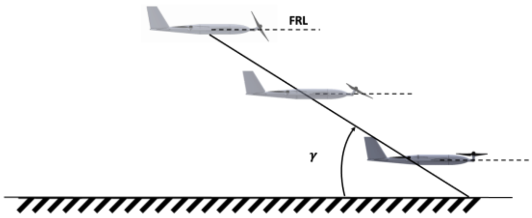

Figure 35: Measurement of descent angle with reference to the horizon

Transition Descent Equations

During transition descent, it is possible for the eVTOL aircraft to decelerate in both the horizontal or vertical direction, which is accounted for using the trim force and moment modelling module. Similarly, for this study, the lift from the tail is assumed small and negligible.

The forces in the vertical axis and horizontal axis must be in equilibrium respectively, that is calculated using Equation (31) and Equation (32). While the summation of all moments acting about the CG, due to the moment arm of the thrust of the rotors is calculated using Equation (33) .The resultant moment must be zero to ensure that the aircraft is not pitching and the fuselage reference line is parallel to the horizon to achieve the vertical landing, while the pitch angle is the equal to the descent angle for a non-vertical landing.

$$\sum T_{z_{rotor_i}} + L_{wing_z} + D_{wing_z} - W_{eVTOL} = m_{eVTOL} \times a_z \quad (31)$$

$$\sum T_{x_{rotor_i}} + L_{wing_x} - D_{wing_x} = m_{eVTOL} \times a_x \quad (32)$$

$$\sum T_{z_{rotor_i}} \times \text{Distance from CG} = 0 \quad (33)$$

Transition Descent Kinematics

To model the transition descent, this study uses the defined trajectory function and kinematics variables such as, distance, velocity, and acceleration. The results generated for the vertical and horizontal axis are shown in Figure 36 respectively.

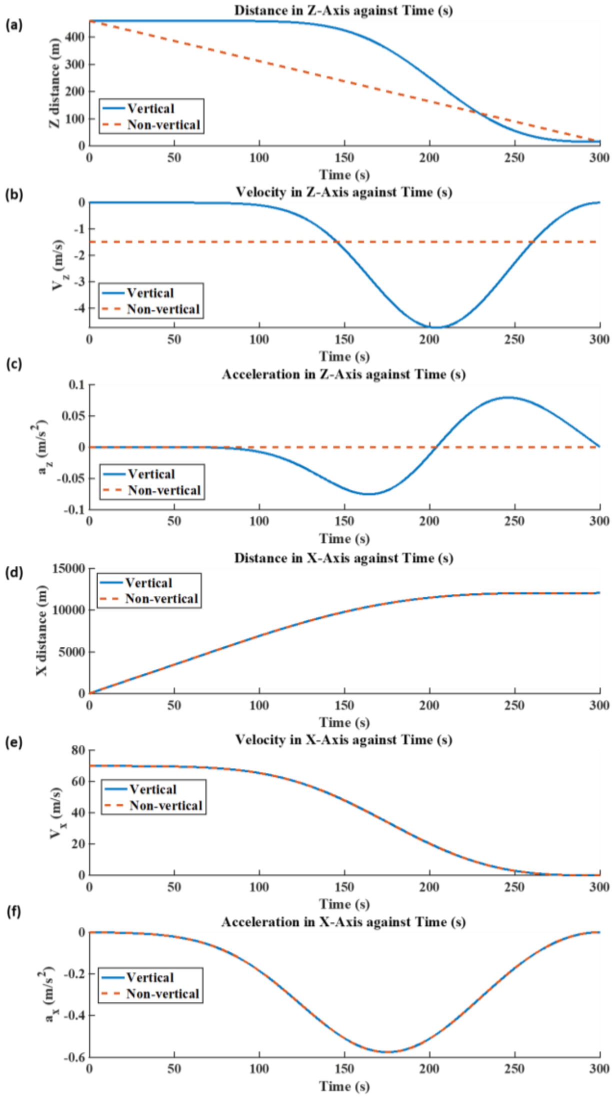

Figure 36: Transition descent results against time for: (a) vertical translation; (b) vertical velocity; (c) vertical acceleration; (d) horizontal translation; (e) horizontal velocity; (f) horizontal acceleration.

The descent angle and the resultant velocities are calculated using Equations (10) and (12). The overall trajectories for both vertical and non-vertical landing are shown in Figure 37 (c). From Figure 37 (a), the descent angle for the both the vertical and non-vertical landing starts from zero, and eventually increases negatively to a larger descent angle. Using the airfoil data from Figure 10, the lift and drag coefficients are matched against the descent angle of the eVTOL aircraft as shown in Figure 38.

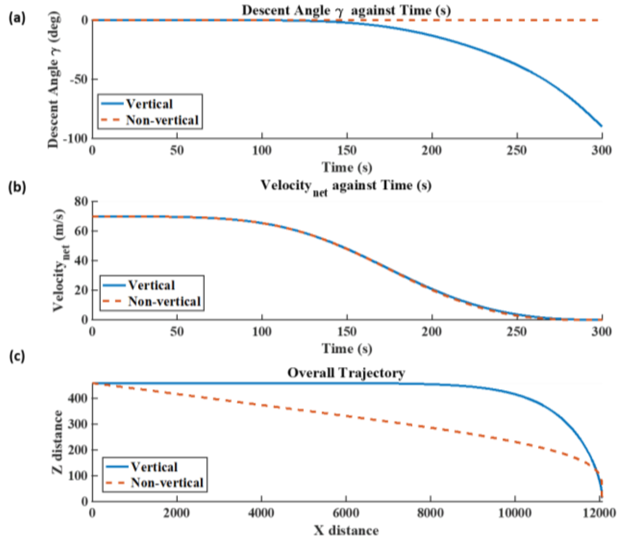

Figure 37: Transition descent results against time for: (a) descent angle; (b) resultant velocity; (c) overall trajectory.

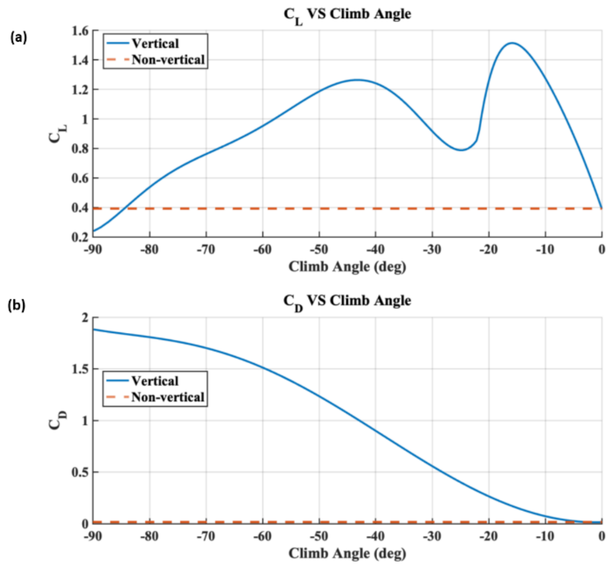

Figure 38: Transition descent results against descent angle for: (a) lift coefficient; (b) drag coefficient.

For the vertical landing transition descent, the trajectory function used is the reflection about the y-axis of the transition climb. During vertical landing, the thrust from the rotors comprises of the vertical and horizontal components, which is used to support the weight and overcome the opposing vertical drag component as shown in Figure 39 (a). Due to the horizontal and vertical velocity components acting on the aircraft, there is an induced descent angle for the resultant velocity, whereby the resultant velocity is used to calculate the lift and drag forces.

The descent angle induces a positive angle of attack on the airfoil. The lift coefficient becomes more positive with a positive angle of attack value, as seen in Figure 10. Thus, only the positive lift coefficient is generated for the vertical landing trajectory as shown in Figure 38 (a).

For the non-vertical landing transition descent, the difference compared to the vertical descent is the orientation of the eVTOL aircraft as shown in Figure 37 (c). The difference between the non-vertical and vertical landing is that the eVTOL aircraft pitches downward during the descent to be aligned with the glide slope, similar to a conventional aircraft, as shown in Figure 34. Hence, the descent angle for this study is shown in Equation (34) and (35).

$$\text{Descent Velcoity} \approx \frac{457.2-15.24}{300} = 1.47 \text{ m/s} \quad (34)$$

$$\text{Descent angle} = \tan^{-1}\left(\frac{1.47}{50}\right) = 1.68° \quad (35)$$

During the transition descent phase in non-vertical landing, the eVTOL aircraft is pitched forward to descent with the forces and velocity components shown in Figure 39 (b). This becomes a controlled landing in which the vertical velocity is assumed to be very small, resulting in a small descent angle, which the eVTOL aircraft resultingly pitches forward slightly such that the fuselage reference line is parallel to the wind reference frame.

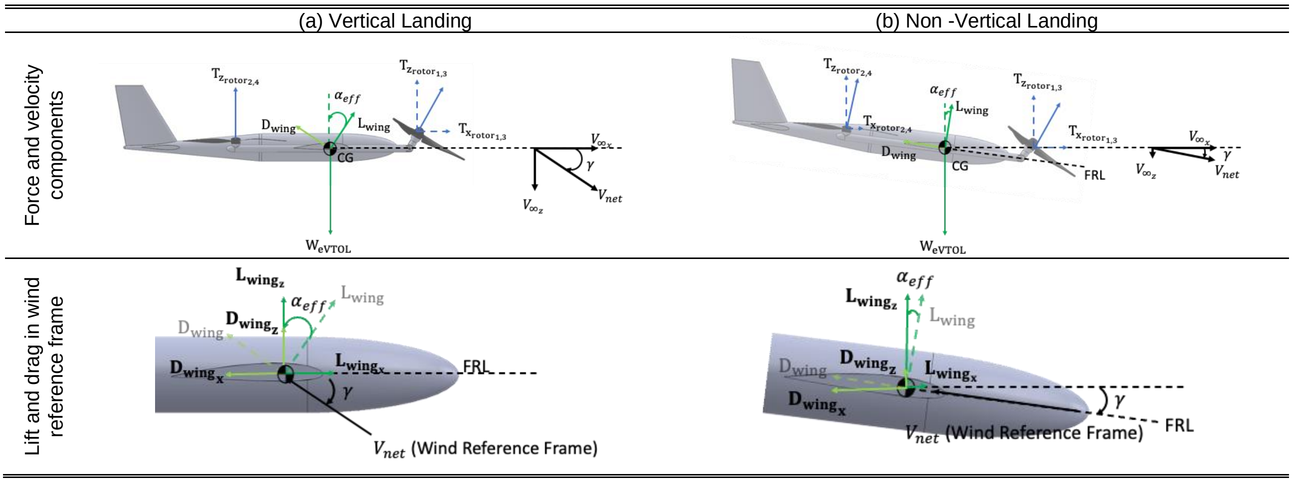

Figure 39: Forces on an eVTOL aircraft and velocity components for a transition descent

Transition Descent Forces

At the start of vertical landing transition descent, the opposing force in the vertical direction, which is made up of two components: (1) lift component and (2) drag component shown in Figure 40 (b), is constant at a high value, while the rotors are not providing any thrust as shown in Figure 40 (a). The opposing force decreases at 75 seconds point, and the rotors compensates the decrease in vertical forces by generating the required thrust accordingly.

From Figure 40 (b), the lift component is the major contributing component to the overall opposing force, due to the difference in its magnitude. At the start of the descent, the wing is still generating lift that is used to support the eVTOL aircraft weight. As the eVTOL aircraft begins to slow down, the net resultant velocity decreases. Hence, the lift component generated gradually decreases resulting in the rotors having to generate required thrust.

The thrust generated by the rotors is used to overcome the opposing force of the eVTOL aircraft in the horizontal direction as shown in Figure 41 (a), which is made up of the lift component and drag component shown in Figure 41 (b). The magnitude of the thrust of the rotors decreases along with a decrease in magnitude of the opposing force, and the magnitude of the rotor thrust increases along with an increase in magnitude of the opposing force. The rotor thrust enters the negative region to slow the eVTOL aircraft for a transition descent in vertical landing trajectory as shown in Figure 41 (a).

For the non-vertical landing transition descent, the opposing force in the vertical direction is mainly influenced by the lift force, as shown in Figure 40 (b). Due a small descent angle for the eVTOL aircraft during non-vertical landing trajectory as shown in Figure 39 (b), the drag component in the vertical component is very small. The changes in lift force are only due to the decrease in velocity. As such, the opposing force and the lift force is a smooth curve, resulting in a smooth increase for the thrust required by the rotors in the vertical direction.

The non-vertical landing opposing force in the horizontal direction is mainly influenced by the drag force as shown in Figure 41 (b). Similarly, the lift component in the horizontal component is very small as shown in Figure 39 (b). The change in drag force is only due to the decrease in velocity, resulting in a smooth curve for the drag force and the opposing force is, and a smooth increase for the thrust required by the rotors in the horizontal direction.

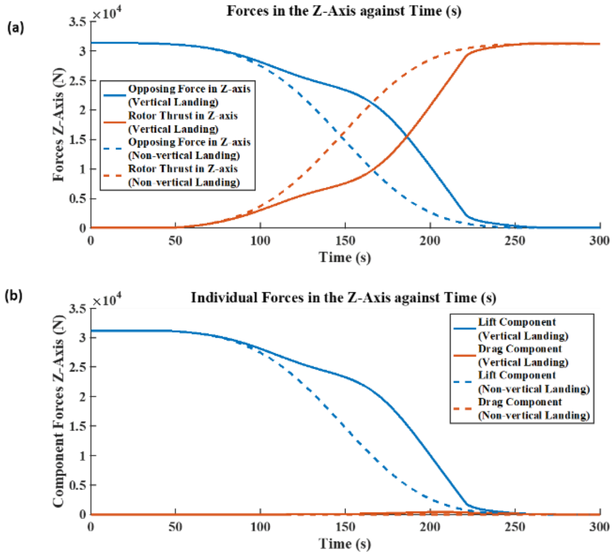

Figure 40: Transition descent results against time for: (a) vertical rotor thrust and opposing force; (b) vertical lift and drag components.

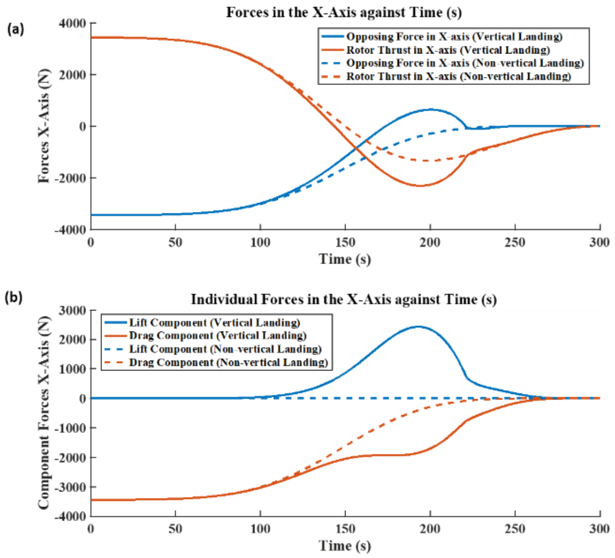

Figure 41: Transition descent results against time for: (a) vertical rotor thrust and opposing force; (b) vertical lift and drag components.

Transition Descent Power Required

During the change between the cruise to transition descent phase, the total power required increases during this trajectory, as shown in Figure 42. This is because the rotors must provide thrust to support the aircraft weight during the transition descent phase. For both vertical and non-vertical landing, the lift-rotors are in idle at the start of the transition descent. As the aircraft decelerates, the lift-rotor power required increases as the total vertical thrust required is being transferred from the wing to the lift-rotors, while the power required by the tiltrotor decreases. This is a result of the decrease in horizontal thrust required for the aircraft to decelerate descent. Subsequently, the power required for the tiltrotor increases as the aircraft slows down further, this is because the tiltrotor has to provide thrust in the vertical direction to support the aircraft weight, as well as to decelerate the aircraft. Due to the changes in the power required by the tiltrotor during transition descent, this results in a noticeable ‘power bucket'.

When comparing the power required curves, the non-vertical landing is smoother than the vertical landing. This is due to the smoother thrust required curve in the vertical and horizontal direction as seen in Figure 40 and Figure 41. The result also shows that the total power required for the transition descent is lower for the vertical landing than the non-vertical landing, allowing for lower power requirements from the electric components.

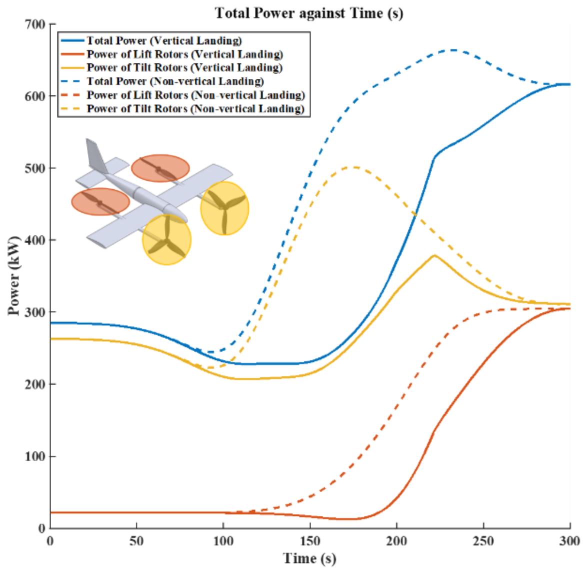

Figure 42: Transition descent - total power, power of lift-rotors and power of tit rotors against time

The shaft angle increases as the tiltrotor is required to provide thrust to support the weight of the eVTOL aircraft, as shown in Figure 43. A unique feature for tiltrotors configurations, it allows the tiltrotor to tilt backwards for a short period to decelerate the aircraft during a transition descent for a vertical landing trajectory. The shaft angle trend between both the vertical and non-vertical landing is very similar, except for the angle at which the extent to which the tiltrotor tilts backward for horizontal deceleration.

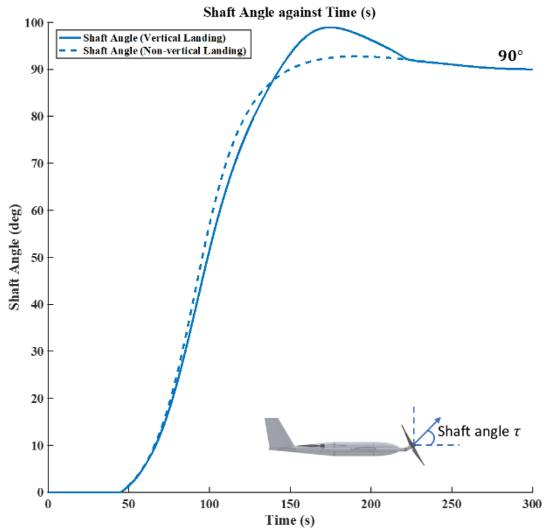

Figure 43: Transition descent - shaft angle of the front tiltable rotor against time.

3.2.3 Combined Power Required and Energy Used for a Main Mission Profile

The overall power required curve for a general main mission profile for the generic eVTOL aircraft is shown in Figure 44. It is shown that the power requirement is lower for a main mission with vertical landing than non-vertical landing transition descent.

In vertical landing, the eVTOL aircraft is levelled and parallel to the horizon, allowing the wing of the aircraft to maintain the lift generated for a longer period of time due to the positive angle of attack induced by the descent angle as shown in Figure 45 (a). In comparison, as the eVTOL aircraft is pitched forward during a non-vertical landing, the wing is not able to maintain the lift generated as it is more sensitive to a velocity change as shown in Figure 45 (b). As a result, the rotor is less burdened to provide thrust to support the weight of the eVTOL aircraft for a vertical landing than a non-vertical landing. Thus, the power required for vertical landing is lower than that of non-vertical landing.

This result is used to estimate the energy usage for the test model for a general main mission profile. The energy usage is split into two components: (1) for cruise flight phase and (2) for non-cruise flight phase. Based on the energy for the cruise phase, the range of the test model can be estimated using Equation (36). The energy usage for the generic eVTOL model is shown in Table 6.

$$\text{Range} = \frac{\text{Energy for Cruise}}{\text{Power required for cruise}} \times \text{Cruise Velocity} \qquad (36)$$

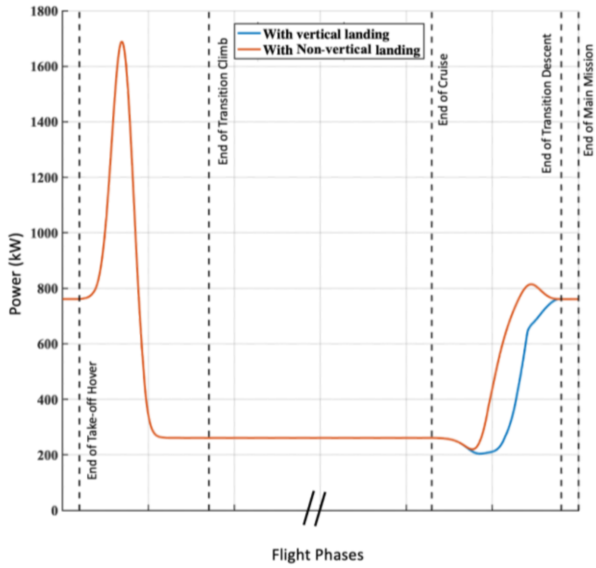

Figure 44: Power requirement for each of the flight phases of a general main mission for a generic eVTOL aircraft with different transition descent model.

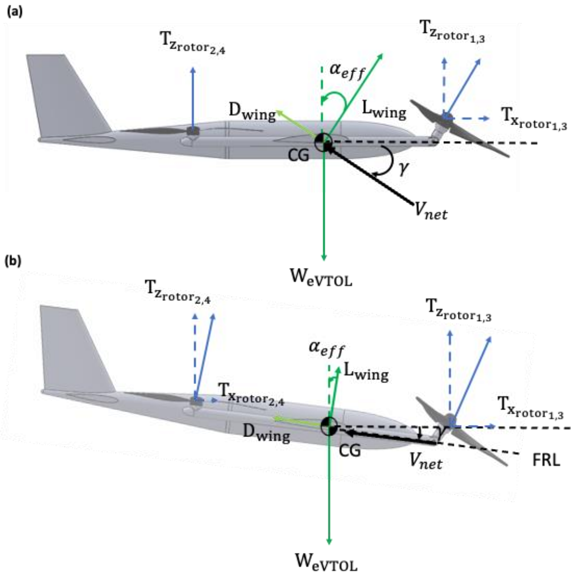

Figure 45: Forces on eVTOL aircraft for (a) vertical landing and (b) non-vertical landing.

From Table 6, non-vertical landing uses up more energy than vertical landing for the transition descent, resulting in a shorter range for the former than the latter, which is in line with the power requirement results as shown in in Figure 44.

Table 6: Energy used in cruise and non-cruise phases and the range of a general main mission profile test model.

	Vertical landing	Non-vertical landing
Total Energy	230 kWh	230 kWh
Cruise Velocity	70 m/s	70 m/s
Range	150.4 km	143.2 km
Cruise	68.7%	65.4%
Non-cruise	31.3%	34.6%

From this study, it can be concluded that regardless of the trajectory that is set for the eVTOL aircraft during the transition descent, the power required for the transitional phases are highly dynamic, and the power required are constantly changing with time as shown in Figure 44. This is essential in sizing the motors for an eVTOL aircraft. Without proper consideration on how the transition might affect the power requirements, an eVTOL aircraft might not be able to achieve the desired trajectory that has been set for it during transition. As a result, this might affect the certification process for the eVTOL aircraft, whether it is able to comply with the regulatory standards set for the transition of the eVTOL aircraft. Hence, this highlights the importance of the trajectory studies for an eVTOL aircraft.

3.3 Effect of eVTOL Configuration on the Power and Aircraft Trajectory

In this final study, the effect of the power requirements and flight performance parameters for a given trajectory was studied for three leading eVTOL aircraft with different configurations, consisting of a Tiltrotor, Lift + Cruise and a Lift + Tiltrotor, with their parameters shown in

Table 8. For each eVTOL aircraft configuration, there is ideally an optimal trajectory to either achieve maximum range or minimum power required. However, in line with regulations, the eVTOL aircraft mission is assumed to follow a standard vertical take-off approach for the transition climb trajectory and a standard vertical landing approach for the transition descent trajectory. As for the Lift + Cruise aircraft, which does not a have tiltable rotor for deceleration, a non-vertical landing approach is assumed for its transition descent trajectory, where the rotors are fixed vertically in position for this configuration.

As such, in this study, the basis for the performance comparison of the three different configurations of eVTOL aircraft, consist of a common mission profile with the: (1) hover, (2) transition climb, (3) cruise, (4) transition descent, (5) landing. Furthermore, assumptions used for BEMT in this study, includes the standard values for the correction factor for power calculations, rotor tip speed, as well as rotor blade drag coefficient as defined in Table 7. The input parameters for the comparison of the three different configurations are shown in Table 9, including the aircraft specifications and the previously calculated fuselage drag coefficient in [4].

Table 8: Different eVTOL configuration used for comparison.

eVTOL (A):	eVTOL (B):	eVTOL (C):
Lift + Cruise E.g., Beta Technologies, *Beta Alia-250* [12]	Tiltrotor E.g., Joby Aviation, *JA S4-1* [13]	Lift + Tiltrotor E.g., Vertical Aerospace, *VA-X4* [14]
		

Transition Climb Power Required Comparison

The power required for eVTOL (A) is the highest, followed by eVTOL (C), and eVTOL (B), as shown in Figure 46. eVTOL (B) has the lowest power required due to it lower weight resulting in a lower disk loading, as compared to the other models. The number of rotors used for hover for eVTOL (A) is less than that for eVTOL (C), as seen in Table 10. Thus, the thrust is distributed among more rotors for eVTOL (C), as a result reducing the induced power required.

Table 9: Input Parameters used for each eVTOL aircraft configuration for trajectory analysis.

Parameters	eVTOL (A)	eVTOL (B)	eVTOL (C)
Configuration Type	Lift + Cruise	Tiltrotor	Lift + Tiltrotor
Total Mass (kg)	3175	2177	3175
Wingspan (m)	15.2	10.5	15
Wing Area (m^2)	19.8	11.6	26.8
Number of Tiltrotors (Primary Rotors)	0	6	4
Number of Pusher Rotors (Primary Rotors)	1	0	0
Number of Lift-rotors (Secondary Rotors)	4	0	4
Primary Rotor Diameter (m)	3.9	3.1	3.1
Number of Rotor Blade for Primary Rotor	3	5	5
Secondary Rotor Diameter (m)	2.15	-	3.3
Number of Rotor Blade for Secondary Rotor	2	-	2
C_{d_0} for Rotor Blade	0.012	0.012	0.012
Rotor tip speed (m/s)	182.88	182.88	182.88
$C_{d_{fuselage}}$	0.0255	0.022	0.020
Available Energy (kWh)	230	160	230

For the power requirements during the transition climb, the power required increase for eVTOL (A) is lesser than both eVTOL (B) and eVTOL (C). This is due to the difference in the number and size of the rotor system. For eVTOL (B) and eVTOL (C), the tiltrotors in the rotor system are responsible for providing thrust in both the vertical and horizontal direction, whereas for eVTOL (A), the lift-rotors and pusher rotors are individually responsible for providing thrust in the vertical and horizontal direction respectively. Hence, by having a distributed rotor system to provide thrust in the different axes, it creates lesser burden on the rotor system. As a result, the power required increase is lesser for eVTOL (A) than the other two configurations, which is a benefit of a Lift + Cruise configuration during the transition climb segment.

Table 10: Comparison of power requirement during hover and cruise between eVTOL (A), eVTOL (B) and eVTOL (C).

Configuration	eVTOL (A)	eVTOL (B)	eVTOL (C)
Mass (kg)	3175	2177	3175
Number of Rotors used for Hover	4	6	8
Power to Hover (kW)	644.7	409.7	576.1
Number of Rotors used for Cruise	1	6	4
Power to Cruise (kW)	239.8	196.1	284.2

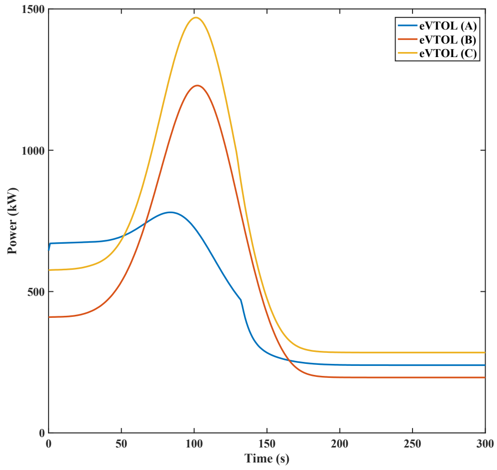

Figure 46: Comparison of power requirement for transition climb between eVTOL (A), eVTOL (B) and eVTOL (C).

Comparing the power to cruise, eVTOL (C) requires the most power, followed by eVTOL (A) and eVTOL (B). Since the weight of eVTOL (B) is the lowest among the aircraft, the wing surface of eVTOL (B) does not require to generate as much lift resulting in a lower induced drag from the wing surface. While eVTOL (C) requires the most power as there is a higher number of rotors used for cruise than for eVTOL (A); 4 tiltrotors compared to 1 pusher rotor respectively as shown in Table 9, which are used during the cruise flight phase of the eVTOL aircraft. Besides that, the tiltrotors of eVTOL (C) uses 5 blades, whereas the pusher rotor of eVTOL (A) uses 3 blades. Thus, there is a higher profile power incurred by eVTOL (C) than eVTOL (A), resulting in a higher cruise power required for eVTOL (C) than eVTOL (A).

Transition Descent Power Required Comparison

During the transition descent, eVTOL (B) exhibits the largest power required spike from cruise power to peak power, as shown in Figure 47. This is because all 6 rotors on eVTOL (B) tilts with all 6 rotors incurring a high-power requirement during the transition descent as all rotors has to provide thrust in both the vertical and horizontal direction.

For eVTOL (A), there is a power bucket as shown in Figure 47. This is a result from the decrease in power required for the pusher rotor and an increase in power required from the lift-rotors. As lesser thrust in the horizontal direction is required for a descent, and a higher thrust is required in the vertical direction when the wing lift is insufficient to support the weight of the aircraft during the descent, hence the lift-rotors are required to support the aircraft during the descent.

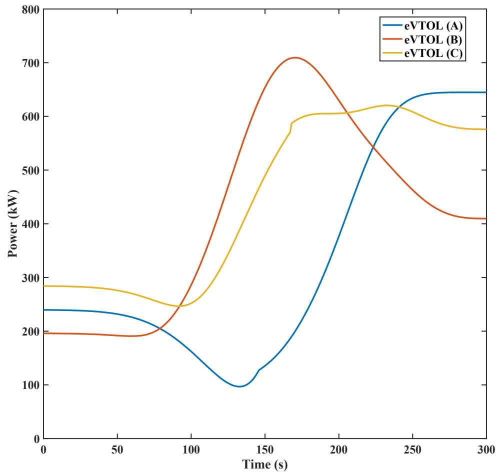

Figure 47: Comparison of power requirement for transition descent between eVTOL (A), eVTOL (B) and eVTOL (C).

Similarly, eVTOL (C) has a power bucket as shown in Figure 47. This is the result of the changes in thrust required for the tiltrotors, and an increase in thrust required for the lift-rotor. Ultimately, it is reflected in the power required for eVTOL (C). Therefore, there is a presence of a power bucket.

During the end of the transition descent, eVTOL (A) and eVTOL (C) requires more power than eVTOL (B) due to difference in weight of the eVTOL aircraft. eVTOL (A) requires greater power than eVTOL (C), due to the lower distributed thrust, resulting in higher induced power for eVTOL (A) than eVTOL (C) at the end of transition descent.

Comparison of Power Required for a complete Mission Profile

The power requirement for a general mission for all three configuration is shown in Figure 48. The transition climb, and transition descent are observed to be highly dynamic when compared to the other flight phases within the main mission regardless of the configuration of the eVTOL aircraft.

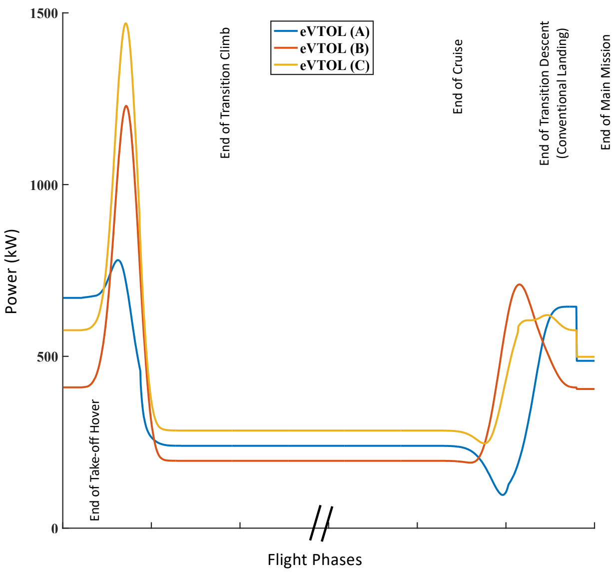

Figure 48: Comparison of power requirement for a general main mission between eVTOL (A), eVTOL (B) and eVTOL (C).

Comparison of Energy and Range for a complete Mission Profile

The distribution of energy for cruise and non-cruise segment for a general main mission for the different eVTOL aircraft configurations is shown in Table 11. eVTOL (A) has the longest range, as the energy available for cruise is the highest compared to the other eVTOL aircraft configurations. This suggest that a Lift + Cruise is more energy efficient in the transitional fight phase. On the other hand, the energy available for cruise is slightly greater for eVTOL (C) than eVTOL (B), resulting in eVTOL (C) having a longer range than eVTOL (B). This is a result of having a smaller total energy for eVTOL (B) than eVTOL (C).

One major assumption used in the calculations is for the rotor tip speed for all eVTOL aircraft configuration remains constant in this study. In reality, each eVTOL aircraft configuration, based on its rotor system and the flight phase may have a different rotor tip speed to optimize for the power required and energy usage. However, as this study is focused on the performance characteristics of different configuration of eVTOL aircraft for a main mission profile with transitional phase, a common rotor tip speed is used, and the results are collected and discussed accordingly. Based on the results collected, it shows that a Lift + Cruise configuration aircraft has benefits in its performance characteristic. A pusher rotor and lift-rotor system help to elevate the burden of having to provide thrust in both the horizontal and vertical direction that a tiltrotor is required to perform. The high-power requirement for tiltable rotor from this study is also align with the first study whereby tilting the rotors will incur a higher power requirement.

Table 11: Distribution of energy used in cruise and non-cruise phases and the range of a general main mission profile for eVTOL (A), eVTOL (B) and eVTOL (C)

	eVTOL (A)	eVTOL (B)	eVTOL (C)
eVTOL Mass (kg)	3175	2177	3175
Total Energy (kWh)	230	160	230
Cruise Velocity (m/s)	70	70	70
Range (km)	184.3	124.2	139.9
Cruise Energy (%)	77.4	62.2	69.6
Non-cruise (%)	22.6	37.8	30.4

4. CONCLUSION

Transition modelling is crucial for the eVTOL aircraft design and its certification as the transition phase is highly dynamic and constantly changing, being a stark difference from hover and cruise phase that is assumed to be at a steady state condition. Moreover, it is essential to meet the regulatory standards and safety guidelines for transition, to ensure a safe operation and comfortable trajectory from one flight phase to another flight phase. This prompt a deep dive into modelling of the transition phase of an eVTOL aircraft. As such, the modelling focuses on three main modules that were further developed to encapsulate the transition flight phase, which are: (1) power required; (2) trim force and moment; (3) kinematic and trajectory. Together with the improved aerodynamics module, these modules are used to conduct three distinct studies.

In the first study, the effects of tilt angle on the lift contribution of the wing were explored. It has shown that having a tilting rotor is beneficial for an eVTOL aircraft, as it allows the wing to generate positive lift for a large velocity range while allowing for an eVTOL aircraft to reach a higher maximum velocity. However, a tiltrotor configuration has a higher power consumption during the phase of tilting its rotors forward.

In the second study, the different individual transition trajectory was investigated. The study has shown that between the vertical and non-vertical landing descent, the total power for the transition descent is lower for the vertical landing than the non-vertical landing, allowing for lower power requirements from the electric components. Moreover, it has shown that the influence of the different trajectories impacting the performance characteristics, in terms of the power requirement, energy usage and the shaft tilt angle of an eVTOL aircraft.

Lastly, a comparison study was carried out between three different configurations of eVTOL aircraft, such as Lift + Cruise, tiltrotor and a combination of Lift + Cruise and tiltrotor. The study shows that a Lift + Cruise configuration is more energy efficient and incurs a lower power limit during the transition phase. The study has also shown that higher power is required for a tiltrotor which is in line with the results in the first study.

Hence, this paper presents a deeper understanding of the intricacy of the transition phase for an eVTOL aircraft. Ultimately, this research work on the transitional characteristics and flight trajectory of different eVTOL aircraft configurations aims to determine an optimal eVTOL configuration in terms of performance while meeting the safety guidelines and regulations.

5. ACKNOWLEDGEMENTS

This research is supported by A*STAR under its MTC IAF-PP (M23L5a0019) and Nanyang Technology University grant 04INS000453C160.

6. REFERENCES

[1] EASA. "Special Condition for VTOL and Means of Compliance." EASA. https://www.easa.europa.eu/en/document-library/product-certification-consultations/special-condition-vtol (accessed June 23, 2023).

[2] Z. Lovering. "Vahana Configuration Trade Study — Part I." Airbus. https://acubed.airbus.com/blog/vahana/vahana-configuration-trade-study-part-i/ (accessed June 23, 2023).

[3] W. Johnson, C. J. Silva, and E. Solis, "Concept Vehicles for VTOL Air Taxi Operations," 2018.

[4] L. K. Y. Shawn, K. J. H. Andy, and W. James, "A Simplified Model for Evaluating eVTOL Conceptual Designs and with Example Results for Three Types of eVTOL Aircraft Configurations," presented at the European Rotorcraft Forum, Switzerland, 2022.

[5] S. S. Chauhan and J. R. R. A. Martins, "Tilt-Wing eVTOL Takeoff Trajectory Optimization," *Journal of Aircraft,* vol. 57, pp. 93-112, 2020.

[6] E. Senkans, M. Skuhersky, B. Kish, and M. Wilde, "A First-Principle Power and Energy Model for eVTOL Vehicles," in *AIAA AVIATION 2021 FORUM*.

[7] U. Elevate. Uber Elevate. https://www.uber.com/us/en/elevate/vision/ (accessed June 23, 2023).

[8] W. Johnson, *Helicopter theory / Wayne Johnson* (no. Accessed from https://nla.gov.au/nla.cat-vn1401694). Princeton, N.J: Princeton University Press, 1980.

[9] W. Timmer and R. Van Rooij, "Some aspects of high angle-of-attack flow on airfoils for wind turbine application," *EWEC Copenhagen, Denmark,* 2001.

[10] W. Johnson. "Lilium e-VTOL achieves new top-speed in test flight." Teslarati. https://www.teslarati.com/lilium-achieves-new-top-speed-155-mph-in-newest-test-flight/ (accessed June 23, 2023).

[11] T. Patterson. "Joby Aviation Claims 'Fastest Flight of an eVTOL Aircraft'." Flyingmag. https://www.flyingmag.com/joby-aviation-reaches-new-top-speeds/ (accessed June 23, 2023).

[12] B. Technologies. Beta Technologies. https://www.beta.team/aircraft/ (accessed June 23, 2023).

[13] J. Aviation. Joby Aviation. https://www.jobyaviation.com/ (accessed June 23, 2023).

[14] V. Aerospace. "Vertical Aerospace VX4." Vertical Aerospace. https://vertical-aerospace.com/vx4/ (accessed June 23, 2023).